ELECTRICAL PROPERTIES OF FROG SKELETAL MUSCLE FIBERS INTERPRETED WITH A MESH MODEL OF THE TUBULAR SYSTEM

R. T. MATHIAS, R. S. EISENBERG, *and* R. VALDIOSERA, *Department of Physiology, UCLA Medical School, Los Angeles, California 90024*

ABSTRACT This paper presents the construction, derivation, and test of a mesh model for the electrical properties of the transverse tubular system (T-system) in skeletal muscle. We model the irregular system of tubules as a random network of miniature transmission lines, using differential equations to describe the potential between the nodes and difference equations to describe the potential at the nodes. The solution to the equations can be accurately represented in several approximate forms with simple physical and graphical interpretations. All the parameters of the solution are specified by impedance and morphometric measurements. The effect of wide circumferential spacing between T-system openings is analyzed and the resulting restricted mesh model is shown to be approximated by a mesh with an access resistance. The continuous limit of the mesh model is shown to have the same form as the disk model of the T-system, but with a different expression for the tortuosity factor. The physical meaning of the tortuosity factor is examined, and a short derivation of the disk model is presented that gives results identical to the continuous limit of the mesh model. Both the mesh and restricted mesh models are compared with experimental data on the impedance of muscle fibers of the frog sartorius. The derived value for the resistivity of the lumen of the tubules is not too different from that of the bathing solution, the difference probably arising from the sensitivity of this value to errors in the morphometric measurements.

INTRODUCTION

The tubular system of skeletal muscle fibers (T-system) is a branching network of tubules which arise as invaginations of the sarcolemma and form an irregular spiral (Peachey and Eisenberg, 1975) almost transversely oriented across the fiber. The tubular system includes most of the cell membrane of muscle fibers and traps a significant component of extracellular space within the fiber. It forms the pathway for radial current flow that conducts the action potential from the sarcolemma to the junctions of the sarcoplasmic reticulum and tubular membrane within the fiber. Thus, the tubular system is an essential component of the mechanism of excitation contraction coupling and contributes importantly to most of the electrical properties of mus-

Dr. Mathias and Dr. Eisenberg's current address is: Department of Physiology, Rush College of Health Sciences, Chicago, Ill. 60612.

cle fibers. Two recent reviews (Costantin, 1975; Nakajima and Bastian, 1976) describe our present knowledge of the tubular system in some detail.

To analyze the electrical properties of muscle fibers, it is necessary to construct and test a model of the tubular system. Much work (references can be found in the above-cited reviews) has shown that the lumen of the T-system is in diffusional equilibrium with the extracellular solution. The luminal solution is thus presumably a good conductor of similar composition to the bathing solution. The small cross-sectional area of the tubules and the long path length of the tubular mesh introduce, however, a significant resistance to radial current flow (Adrian, Costantin and Peachey, 1969). The most widely used model of the tubular system—the distributed model introduced by Falk and Fatt (1964) and revised and extended by Adrian, Chandler and Hodgkin, (1969), and Schneider (1970)—analyzes the effect of such radial resistance and allows the potential across the tubular membrane to vary with the radial distance from the center of the fiber. To calculate the radial distribution of potential, the distributed, or disk model as we prefer to call it, assumes the branching of the T-system to be very dense. The tubular system is thus described as two parallel disks of membrane with radial potential drops produced by the small volume of the luminal space between the disks. The effect of the branching of the tubules is included in the disk model by the introduction of a tortuosity factor, computed for a few models of the network.

The disk model better describes the electrical properties of muscle fibers than simpler models (Gonzalez-Serratos, 1966; Adrian, Costantin and Peachey, 1969; Schneider, 1970; Hodgkin and Nakajima, 1972*a*,*b*; Barry and Adrian, 1973; Valdiosera et al., 1974*b*,*c*) but it suffers from at least two defects: it seems unable to account for the shape or conduction velocity of the action potential (Adrian and Peachey, 1973), at least without arbitrary modification; and it produces a value of the resistivity of the luminal solution far in excess of that of the bathing solution, when the resistivity is measured by a variety of techniques (Falk and Fatt, 1964; Endo, 1966; Schneider, 1970; Hodgkin and Nakajima, 1972*a*,*b*; Valdiosera et al., 1974*c*; Nakajima et al., 1975). The former defect can perhaps be explained by our lack of knowledge of the nonlinear properties of the tubular membrane and T/SR junction; the latter defect is more difficult to explain, particularly in view of the finding of Gilai (1976) that the resistivity of the luminal solution in muscle fibers with *unbranched* tubules is equal to that of the bathing solution. The disk model suffers another less serious defect. When there is significant decrement of potential within a single tubular branch, the density of branching clearly cannot be assumed to be infinite. In this case the disk model cannot be used to describe the properties of the T-system.

For these reasons it seemed useful to construct a model of the tubular system that explicitly describes the branching nature of the tubules, a mesh model of the tubular system. Comparison of the continuous limit of the mesh model to the disk model of Adrian et al. (1969*a*) shows that, in the limit, they have the same form, but with a different expression for the tortuosity factor. A revised derivation of the disk model, however, gives results in agreement with the limit of the mesh model. The mesh model is shown to fit experimental data on the linear electrical properties of muscle fibers of

fixed length in five solutions of normal tonicity. The validity of the model can be further tested experimentally by examining its predictions of the nonlinear properties of the muscle fiber, particularly of the action potential. Most importantly, experimental tests can be made of the model by measuring electrical and morphometric properties of muscle fibers in a range of fiber lengths and diameters and in solutions of different tonicities. In the future, the model should be generalized by a theoretical examination of a three-dimensional model of the T-system.

GLOSSARY

Electrical Parameters

C_m^* Capacitance of a unit of sarcolemma, assuming the fiber is an unfolded cylinder (f/cm^2).

c_T Capacitance of the wall of a unit length of tubule (f/cm).

C_W Capacitance of a unit area of tubular wall (f/cm^2).

g_T Conductance of the wall of a unit length of tubule (Ω^{-1}/cm).

G_w Conductance of a unit area of tubular wall ($\Omega^{-1}cm^2$).

i_n^- Total current leaving all nodes in shell n and flowing inward to nodes in shell $n-1$ (A).

i_n^θ Total current leaving nodes in shell n and flowing tangentially toward other nodes in shell n (A).

i_n^+ Total current leaving nodes in shell n and flowing outward to nodes in shell $n+1$ (A).

$i_{n,k}^-$ Current leaving a node in shell n and flowing in branch k, where branch k connects nodes in shell n and shell $n-1$ (A).[1]

$i_{n,k}^\theta$ Current leaving a node in shell n and flowing in branch k, where branch k connects between nodes in shell n (A).[1]

$i_{n,k}^+$ Current leaving a node in shell n and flowing in branch k, where branch k connects k connects nodes in shell n and shell $n+1$ (A).[1]

i_r Radial current in a disk model of the T-system (A).

$\underline{r}$ DC resistance in a unit length of fiber due to the sarcolemma and T-system membrane (Ωcm).

r_a Effective access resistance in a unit length of fiber due to a wide circumferential spacing of openings to the tubular mesh (see Eq. 49) (Ωcm).

R_B Resistivity of the bathing solution (Ωcm).

r_i Resistance of the sarcoplasm in a unit length of fiber (Ω/cm).

R_i Resistivity of the sarcoplasm (Ωcm).

r_{iT} Resistance of the luminal solution in a unit length of tubule (Ω/cm).

$\tilde{R}_L$ "Resistivity" of the volume of tubular lumen contained in a unit volume of fiber (see Eq. 51) (Ωcm).

$\tilde{R}_L$ Resistance of the volume of tubular lumen contained in a unit area of one Z-disk (see Eq. 52) (Ω).

R_{rad} Effective resistance to radial current flow in a single Z-disk (see Eq. 50) (Ω).

$U(r, j\omega)$ Potential drop across the tubular wall at radius r (V).

$U_n(j\omega)$ Potential drop across the tubular wall at a node in the n^{th} shell (V).[1]

---

[1] These parameters also appear in the text in boldface type as random variables. A random variable represents an ensemble (i.e. set) of parameters, each parameter having the given definition.

$V_m(x,j\omega)$ Potential drop across the sarcolemma (V).

$Y_n(j\omega)$ Admittance of a mesh looking inward from all the nodes in shell n (Ω^{-1}).[1]

$\tilde{y}_n(j\omega)$ Admittance of a mesh looking inward from one node in shell n (see Eq. 42), (Ω^{-1}).

$y_{rm}(a,j\omega)$ Admittance in a unit length of fiber due to a T-system which has a restricted number of openings to the bathing solution (Ω^{-1}/cm).

$y_T(a,j\omega)$ Admittance of the T-system in a unit length of fiber (Ω^{-1}/cm).

$Y_T(a,j\omega)$ Admittance of the T-system associated with a unit area of fiber surface (Ω^{-1}/cm^2).

$Y_{TO}(j\omega)$ Characteristic admittance of a single tubule (Ω^{-1}).

$y_{11}(L,j\omega)$ The 1, 1 element of the short circuit admittance matrix for a tubule; see Fig. 1 where $y_{11} = I_{in}/U_{in}$ with $U_{out} = 0$; also see Eq. 3 (Ω^{-1}).

$y_{12}(L,j\omega)$ The 1, 2 element of the short circuit admittance matrix for a tubule; see Fig. 1, $y_{12} = I_{out}/U_{in}$ with $U_{out} = 0$; see also Eq. 4 (Ω^{-1}).

$\tilde{y}_\infty(j\omega)$ Admittance of a mesh looking inward from one node located at an infinite radius; see Eq. 40. (Ω^{-1}).

$\Gamma(j\omega)$ Propagation constant for a single tubule. At DC (i.e. $j\omega = 0$), Γ is the reciprocal of the length constant; see Eq. 5, (cm^{-1}).

$\Gamma_m(j\omega)$ Effective propagation constant for a mesh of tubules. At DC (i.e. $j\omega = 0$) Γ_m is the reciprocal of λ_T; see Eq. 28, (cm^{-1}).

λ_T Effective DC length constant for a mesh of tubules, (cm).

τ_f Time constant determined from the foot of the action potential (s).

$\psi_m(j\omega)$ An approximate solution to the potential drop across the tubular wall at a node in the n^{th} shell; see Eq. 37, (V).

Mathematical Parameters

$j\omega$ The Fourier transform parameter where $j = \sqrt{-1}$ and ω has the physical interpretation of angular frequency in radians per second.

J_n The number of radial tubular branches joining nodes in shell n with nodes in shell $n-1$.[1]

K_n The number of tubular branches joining nodes in shell n with other nodes in shell n.[1]

M_n The number of radial tubular branches joining nodes in shell n with nodes in shell $n+1$.

R A unitless measure of the radius of a mesh normalized by the effective propagation constant of the mesh; see Eq. 27.

R_{test} A statistical measure of the goodness of fit of a theoretical curve to a set of data.

ξ A unitless parameter defined in Eq. 19, which arises as the natural argument in the solution to the difference equations; intuitively $\xi = \Gamma_m \Delta r$.

ξ_o A unitless convenient combination of morphometric parameters (see Eq. 41).

ρ The ratio $(-y_{11}/y_{12})$; for a tubule this is cosh (ΓL).

Morphometric Parameters

a Fiber radius (cm).

L Average length of a tubular branch (cm).

L_T/A_F Average length of tubules in a unit area of Z disk (cm^{-1}).

L_T/V_F Average length of tubules in a unit volume of fiber (cm^{-2}).

N_B Average number of branches per node in the T-system.

r Radial distance within a circular mesh (cm).

Δr Average distance between shells in a mesh (see Eq. 26) (cm).

S_T/A_F Average surface area of tubular wall in a unit area of Z disk.

---

[1]These parameters also appear in the text in boldface type as random variables. A random variable represents an ensemble (i.e. set) of parameters, each parameter having the given definition.

S_T/V_F	Average surface area of tubular wall in a unit volume of fiber (cm^{-1}).
S_T/V_T	Average surface-to-volume ratio of a tubule (cm^{-1}).
V_T/A_F	Average luminal volume in a unit area of Z disk (cm).
V_T/V_F	Average luminal volume in a unit volume of fiber.
δ_B	Average distance between radial branches, defined precisely as the circumference of a closed curve of average radius (separating two shells) divided by the number of radial branches connecting the two shells.
δ_N	Average distance between nodes in a shell, defined precisely as the circumference corresponding to the average radius of a shell divided by the number of nodes in the shell.
δ_S	Average circumferential distance between the surface openings of the T-system.
ζ	The part of the tortuosity factor that depends only on the geometry of the interconnection of branches (see Eq. 60).
σ	Sarcomere spacing (cm).
τ	The tortuosity factor, defined explicitly by Eq. 64 or intuitively by Eq. 54.

THEORY

Description of Current Flow in a Tubular Branch

The transverse tubular system is a mesh of current-carrying tubules. Each branch of the tubular mesh can be represented as a miniature transmission line of length L with one-dimensional current flow in the lumen of the tubular branch and "leakage" of current from the lumen to the sarcoplasm through the conductance and capacitance of the wall of the tubules (Fig. 1). The properties of each tubular branch can be described by a differential equation, similar to that used in one dimensional cable theory to describe a cylindrical cell (reviewed by Jack, et al., 1975). It would be unwieldy, however, to describe the properties of the entire tubular mesh as a system of differential equations, one equation for each tubular branch, and so we will use another approach. The differential equation of each tubular branch can be solved for general boundary conditions and the current voltage relations at each end of the branch (or port as it is called in the engineering literature) can be written as a pair of linear algebraic equations. These are the equations of two-port theory (Desoer & Kuh, 1969, Ch. 17) applied to transmission lines (Ghausi and Kelley, 1968, p. 7).

$$I_{in} = y_{11} U_{in} + y_{12} U_{out}; \tag{1}$$

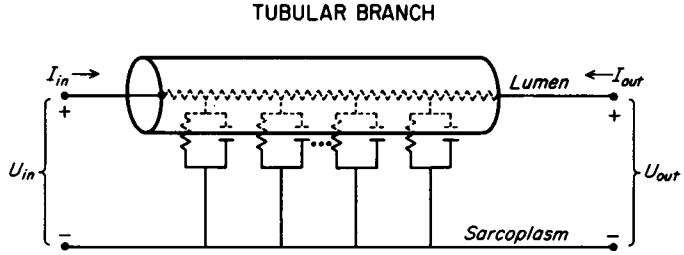

FIGURE 1 The circuit representation of a tubular branch of length L. Each circuit element in the analysis of the mesh model is assumed to be such a distributed network.

$$I_{out} = y_{12} U_{in} + y_{11} U_{out}. \tag{2}$$

The parameters y_{11} and y_{12} are called the short-circuit admittances since they describe, respectively, the complex frequency dependent input admittance I_{in}/U_{in} of the transmission line (see Fig. 1) and the transfer admittance I_{out}/U_{in}, both with $U_{out} = 0$, namely with a short-circuited termination. These parameters can be described in terms of the resistance r_{iT} of a unit length of tubular lumen and the conductance g_T and capacitance c_T of a unit length of wall of tubule.

$$y_{11} = Y_{TO} \coth \Gamma L; \tag{3}$$

$$y_{12} = -Y_{TO}/\sinh \Gamma L. \tag{4}$$

The propagation constant is

$$\Gamma = \sqrt{r_{iT}(g_T + j\omega c_T)} = \sqrt{(S_T/V_T) R_L (G_w + j\omega C_w)}. \tag{5}$$

The characteristic (i.e., input) admittance of a single tubule is

$$Y_{TO} = \sqrt{\frac{g_T + j\omega c_T}{r_{iT}}} = \frac{(S_T/A_F)}{(L_T/A_F)} \frac{\Gamma}{R_L(S_T/V_T)}, \tag{6}$$

where R_L is the resistivity of the lumen of the tubules, G_w and C_w are the conductance and capacitance of 1 cm^2 of tubular wall, S_T/A_F is the surface of tubule per unit cross-sectional area of fiber, S_T/V_T is the surface of tubular wall per unit volume of tubule, and L_T/A_F is the length of tubule per unit cross-sectional area of fiber. The morphometric parameters are introduced in this manner to be consistent with the morphological literature (Mobley and Eisenberg, 1975).

We use the propagation constant to describe the spatial variation of potential instead of the length constant usually used by physiologists, since the propagation constant has a simple meaning for sinusoidal signals whereas the length constant does not: the real part of the propagation constant determines the spatial decrement in the potential, the imaginary part of the propagation constant determines the phase delay in the potential. These relations were first pointed out in the physiological literature by Schneider, 1970.

Analysis of a Class of Random Networks

The tubular system can be described as a random network of circuit elements, each element being a tubular branch. Circuit analysis can be applied to this mesh by considering it as a "network graph" (Desoer and Kuh, 1969, Ch. 9) and applying some elementary statistical ideas to the resulting equations. The derivation presented here is applicable to a rather wide class of random networks, which resemble the tubular mesh, but there are some cases to which it does not apply (see Discussion).

We divide the tubular system into a series of shells by a set of closed curves shown in Fig. 2. The openings of the tubules are considered to be the first set of nodes, special properties of these openings being considered later. A closed curve is constructed to isolate the surface nodes from the next set of nodes. This curve cuts every tubular

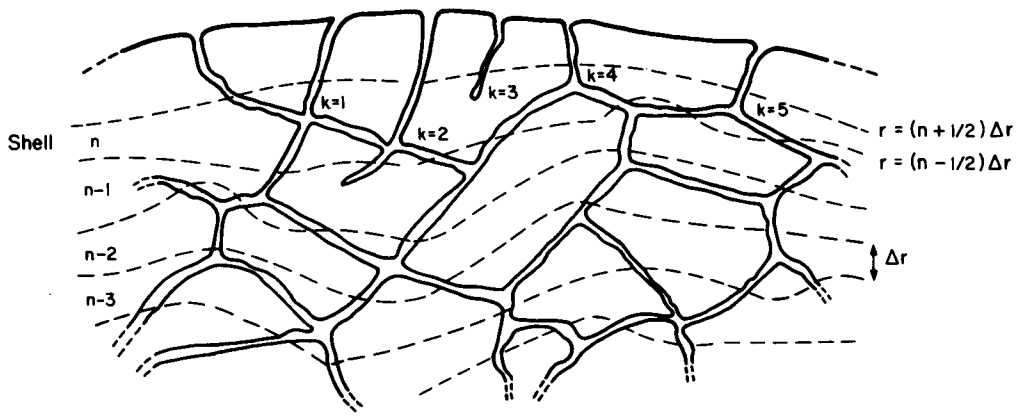

FIGURE 2 The shell construction for an irregular T-system. Each shell, indexed n, $n-1$ ... is defined by "closed" curves shown as dashed lines, the curves on the average being distance $(n+\frac{1}{2})\Delta r$, $(n-\frac{1}{2})\Delta r$, ... from the center of the network. The nodes within the shells are thus on the average $n\Delta r$, $(n-1)\Delta r$, ... from the center. Within each shell the nodes are indexed $k = 1, 2, 3, \ldots$. Note that the end of a blind tubule is considered a node. Tubules cut by a closed curve are called radial branches; those not cut are called θ branches.

branch in the region between the fiber surface and the first node within the fiber. Such branches, cut by the curve, are called radial branches. The next shell inward (labeled shell n in Fig. 2) contains all the nodes with branches extending to the surface. All the nodes within any shell can be indexed as shown for shell n, remembering that the termination of a blind tubule counts as a node. Note that both the $k = 1$ and $k = 2$ nodes are assigned to shell n according to this procedure; thus, the branch connecting them will *not* be cut by any closed curve and must be analyzed somewhat differently from branches which are cut. Such uncut branches are called θ branches.

The definition of shell n specifies the construction of the next deeper closed curve within the network. Equivalently, the next deeper closed curve can be defined as the line that isolates nodes in shell n from nodes further inside the fiber. The shell $n-1$ will contain the set of nodes that connect to shell n; the previously defined process can be repeated until all the nodes have been classified into shells. This construction is uniquely defined, providing each node is connected (as defined in Desoer and Kuh) to the surface and the network is planar. The uniqueness and practicality of the construction have been checked empirically in a number of hypothetical cases. The construction has also been successfully applied to large areas of T-system of real muscle fibers as seen in high-voltage electron micrographs, kindly supplied by L. D. Peachey and B. Eisenberg.

The construction just described is motivated by the following considerations. The potential at the nodes of a circularly symmetric network enclosed in a circular boundary has circular symmetry. Such a circularly symmetric distribution of potential depends on only one independent spatial variable and so is much simpler to analyze than the nonsymmetric case, which must include at least two spatial variables (com-

pare the analysis of the symmetric model [p. 33] and rectangular models [p. 37–51] in Mathias, 1975). We want a construction that will allow an analysis of a random network in terms of a distribution of potential that, when averaged over a set of networks, is circularly symmetric and so, on the average, is only a function of the distance from the center of the network. The closed curves of the construction for an irregular network cannot in general be concentric circles (as they could be for the deterministic circular network) because such curves would not classify nodes of a general random network according to their electrical distance from the surface of the fiber, the electrical distance being equivalent to the number of nodes or radially oriented branches between the node in question and the surface. The construction presented above is designed to produce shells each of which includes all the nodes a given electrical distance from the surface. We expect that this construction, applied to a particular network, will produce a set of shells with the least possible variation of potential from node to node within each shell. Some networks might be so irregular that potential would vary considerably around the circumference of one shell. The potential in such an aberrant network might deviate so considerably from that of a circularly symmetric network that our approach would not be useful. However, in an average network we expect that the potential will be quite symmetrical, with small variance. Our subsequent analysis will therefore assume that the potential can be described by a function of a single spatial variable; in other words subsequent analysis will assume that the potential is circularly symmetric and the outside of the network is a circle. The properties of networks with rectangular symmetry and a rectangular boundary (Mathias, 1975) are remarkably close to networks with circular boundaries, and so we suspect our analysis is more applicable to polygonal fibers than might have been expected.

Derivation of Difference Equations for Current and Potential

The analysis of current flow in the network of shells just constructed requires the systematic identification of each node within each shell. The following nomenclature seems quite simple; the slight ambiguity it allows will disappear as soon as we put the equations into usable form.[2] The current leaving the n, k node in a radial branch connected to a node in the $n - 1$ shell will be called $i^-_{n,k}$. Current leaving the n, k node in a radial branch connected to a node in the $n + 1$ shell will be called $i^+_{n,k}$. The current leaving the n, k node in a θ branch is called $i^\theta_{n,k}$.

At every node in shell n, we have

$$i^-_{n,k} + i^+_{n.k} + i^\theta_{n,k} = 0, \tag{7}$$

and summing over all nodes in that shell, we have

$$\sum_k (i^-_{n,k} + i^+_{n,k} + i^\theta_{n,k}) = 0, \tag{8}$$

[2]Ambiguity arises, for example, when a node in the $n - 1$ shell is connected to more than one node in shell n. The ambiguity disappears as soon as the expected value of the random variables is taken.

or

$$\sum_{j=1}^{J_n} i_{n,j}^{-} + \sum_{m=1}^{M_n} i_{n,m}^{+} + \sum_{k=1}^{K_n} i_{n,k}^{\theta} = 0, \tag{9}$$

where J_n, M_n, and K_n are the total number of each type of branch within shell n. Later we will determine the dependence of these numbers on the shell index n and the morphometric parameters of the tubular mesh.

To analyze these currents, we must use the idea of a random variable as defined in works on probability theory (e.g., Papoulis, 1965). If an ensemble of networks is considered, we can define random variables that represent the three types of current flow. Each such random variable is printed in boldface type and represents the set of all currents which can occur at the nodes index n,k. Similarly, each random variable used later for voltage or admittance describes the set of all such parameters possible at the nodes indexed n,k. In our case the number of each type of branch $\mathbf{J}_n$, $\mathbf{M}_n$, and $\mathbf{K}_n$ are random variables, as are the corresponding currents in each branch. For example, each particular $i_{n,j}^{-}$ in Eq. 9 is the value of the random variable $\mathbf{i}_{n,j}^{-}$, evaluated for a particular node j in some specific network. The random variable $\mathbf{i}_{n,j}^{-}$ thus describes the set of all currents which flow away from a node in a shell indexed n through a branch connected to an $n-1$ shell. Here our interest is in the mean value of the currents in each type of branch and so Eq. 9 must be converted into an equation that describes the mean value of the currents. The expectation operator $E(\cdot)$[3] (Papoulis, p. 138) performs this transformation. For example, applying the operator to the set of all sums in Eq. 9 using a theorem for random sums (Papoulis, p. 248) gives

$$E\left[\sum_{j=1}^{\mathbf{J}_n} i_{n,j}^{-}\right] = E(\mathbf{J}_n)E(\mathbf{i}_{n,j}^{-}) = J_n i_n^{-}, \tag{10}$$

where we have written the symbol J_n for the expected value of $\mathbf{J}_n$ (in shell n) and similarly for the current. Eq. 9 then becomes

$$J_n i_n^{-} + M_n i_n^{+} + K_n i_n^{\theta} = 0. \tag{11}$$

At this point it is useful to introduce some morphometric parameters: N_B, the mean number of branches per node; δ_B, an average spacing between "radial" branches, defined precisely as the circumference of a closed curve of average radius in Fig. 2

[3]When we take expectations in this theoretical analysis, we have in mind one main source of variance, namely the variance of the morphometric and electric parameters within the T-systems of one muscle fiber. This variance arises both from the variation of the parameters of a single tubular branch and from the random connections of the T-system. Another source of variance is the variation of properties from fiber to fiber and muscle to muscle. This is not included explicitly in our analysis. In the Results section this source of variance is handled by the usual techniques of biological experimentation: the experimental data analyzed are collected from a large number of muscles and muscle fibers of generally similar properties. A better technique is, of course, to measure mean electrical and morphometric parameters in the same fiber.

divided by the number of branches cut by the curve; δ_N, the average spacing between nodes defined precisely as the circumference corresponding to the average radius of the shell (evaluated in the middle of the shell) divided by the number of nodes in the shell; and Δr, the average width of a shell. It is important to note that the radius r can be written as $n\Delta r$, but Δr is *not* specified as equal to the branch length L, since we neither require that the mesh be stretched taut, nor do we restrict how the branches are connected within the plane of the network.

The total number of branches can be written as

$$J_n + M_n + K_n = \frac{2\pi(n - \frac{1}{2})\Delta r}{\delta_B} + \frac{2\pi(n + \frac{1}{2})\Delta r}{\delta_B} + K_n, \tag{12}$$

where the number of minus branches J_n has been determined at a distance $(n - \frac{1}{2})\Delta r$ from the center of the fiber and the number of plus branches M_n has been determined at a distance $(n + \frac{1}{2})\Delta r$. A morphometric estimate of K_n, the number of θ branches in shell n, is not available, but K_n can be determined, once the minus and plus branches are counted, from the total number of nodes in the shell n and the average number of branches per node.

$$\frac{2\pi n\Delta r}{\delta_N} N_B = \frac{2\pi(n - \frac{1}{2})\Delta r}{\delta_B} + \frac{2\pi(n + \frac{1}{2})\Delta r}{\delta_B} + K_n. \tag{13}$$

Note that the left-hand side of Eq. 13 is twice the number of branches *contained* in the n^{th} shell, since the θ branches are counted twice (once from each end) and the plus and minus branches are, on the average, half in shell n and half in the adjacent shells. K_n is then given by

$$K_n = \left(\frac{\delta_B}{\delta_N} N_B - 2\right)\left(\frac{2\pi n\Delta r}{\delta_B}\right). \tag{14}$$

Now, if we substitute from Eqs. 14 and 12 into Eq. 11, we get a statement of the current equation in terms of morphometric parameters:

$$(n - \tfrac{1}{2})i_n^- + (n + \tfrac{1}{2})i_n^+ + n\left(\frac{\delta_B}{\delta_N} N_B - 2\right)i_n^\theta = 0 \tag{15}$$

For our purposes we must convert this equation to a description of the potential. We can do this obviously by using the two-port formulation (Eq. 1, 2). for the deterministic case and proceed directly to Eq. 18, but in our present situation, where the currents are random variables, the derivation is somewhat more complex. Consider the currents

$$\mathbf{i}_{n,m}^+ = \mathbf{y}_{11}^m \mathbf{U}_{n,m} + \mathbf{y}_{12}^m \mathbf{U}_{n+1,m}. \tag{16}$$

The expected value of these currents is given by

$$i_n^+ = E(\mathbf{i}_{n,m}^+) = E(\mathbf{y}_{11}^m \mathbf{U}_{n,m}) + E(\mathbf{y}_{12}^m \mathbf{U}_{n+1,m}), \tag{17}$$

where $\mathbf{U}_{n,m}$ represents the set of all nodal potentials in all shells indexed n. The n indexing for the admittances is not included since the expected value of these parameters is assumed to be independent of the location within the network. However, the m index is retained to indicate that the short-circuit admittances always arise in branches incident to the node at which potential is specified. Thus, the potential at a node is more highly correlated with the admittance variable than would be the case if the variable described the set of admittances of all branches.

The derivation of an expression for potential will require the evaluation of several expectations like that shown on the right-hand side of Eq. 17. The evaluations require some analysis since the random variables over which the expectation is to be performed are in general correlated. Appendix I shows that a statistical analysis gives a classical difference equation for the mean potential in the shell N:

$$(n + \tfrac{1}{2})U_{n+1} + (n - \tfrac{1}{2})U_{n-1} - n(2 + \xi^2)U_n = 0, \tag{18}$$

where

$$\xi^2 = \frac{\delta_B}{\delta_N} N_B(\rho - 1); \quad \rho = -y_{11}/y_{12} = \cosh \Gamma L \tag{19}$$

$$\xi^2 = (\Gamma L)^2 \left(\frac{\delta_B}{\delta_N} \frac{N_B}{2}\right)\left(1 + \frac{2}{4!}(\Gamma L)^2 + \frac{2}{6!}(\Gamma L)^4 + \cdots\right). \tag{20}$$

Note that

$$n\xi \to \left(\frac{\delta_B}{\delta_N} \frac{N_B}{2}\right)^{1/2} n\Gamma L \quad \text{as } \Gamma L \to 0. \tag{21}$$

The tubular branch length times the propagation constant is a natural dimensionless parameter to describe the effective branch length. The limiting expression, Eq. 21, in valid only if the effective branch length is small, that is, the branch length is much less than the length constant. Such is the case at DC in most physiological circumstances, but it certainly is not the case either during all experimental procedures or during all natural electrical activity.

The Continuous Limit and the Disk Model of the Tubular System

The analysis presented up to here has been of a discrete network and so it is natural that a difference equation should be the resulting description of the potential in the network. Previous analysis of the properties of the T-system have assumed that the branch length in the t-system is sufficiently small to allow the potential to be approximately described by a differential equation. To compare our analysis with the previous analysis of the disk model of the tubular system, we consider the limiting case of the difference eq. 18. The difference equation can be written:

$$\frac{U_{n+1} - 2U_n + U_{n-1}}{\xi^2} + \frac{1}{\xi n} \frac{U_{n+1} - U_{n-1}}{2\xi} - U_n = 0. \tag{22}$$

The difference equation has been called Bessel's difference equation (Pearson, 1960) since it is a finite difference representation of Bessel's differential equation. The relation of the difference and differential equation can be studied by taking the limit as $\xi \to 0$. We introduce a dimensionless radial coordinate $R = n\xi$, which stays fixed in the limiting process and so becomes the independent variable in the differential equation. The limit can be taken, remembering that U_{n+1} is defined as $U([n + 1]\xi) = U(n\xi + \xi) = U(R + \xi)$, and that the limit $\xi \to 0$ is equivalent to $\Delta R \to 0$, with R fixed.

$$\frac{d^2U}{dR^2} + \frac{1}{R}\frac{dU}{dR} - U = 0 \tag{23}$$

This differential equation describes networks with vanishing branch length, since Eq. 21 shows that the $\xi \to 0$ limit is equivalent to the $L \to 0$ limit. This differential equation is closely related to that of the disk model of the tubular system (Adrian et al., 1969*a*) and will in fact be converted into precisely that form. To complete the analysis, the explicit expression is needed for the relationship of the dimensionless spatial variable R and the physical radial variable r. The ratio of these two variables is defined as a propagation constant Γ_m of the entire tubular mesh:

$$\Gamma_m \triangleq \frac{R}{r} = \frac{n\xi}{r}. \tag{24}$$

Remembering that $n\Delta r \triangleq r$, and using Eq. 21, we have

$$\Gamma_m \to \left[\frac{\delta_B}{\delta_N}\frac{N_B}{2}\right]^{1/2} \Gamma \cdot \frac{L}{\Delta r} \quad \text{as } L \to 0. \tag{25}$$

The above expression does not explicitly determine the propagation constant of the mesh, since in general the branch length L and the shell size Δr are not equal (e.g., Adrian et al., 1969*a*, Fig. 11 *c*).

The relation of L and Δr can be determined directly from measurable morphometric parameters of the network by calculating the total number of branches per shell, both radial and θ branches, in two different ways. The area of a shell of radius r is $2\pi r\Delta r$, and the number of branches per cross-sectional area is $(L_T/A_F)/L$, where L_T/A_F is the length of tubule per unit cross sectional area of mesh. The number of branches per shell is thus $[L_T/A_F][2\pi r\Delta r]/L$. The number of branches per shell is also $[\frac{1}{2}] \times$ [number of nodes/shell] $\times$ [branches per node] $= [2\pi r/\delta_N][N_B/2]$, where the factor one-half arises because each branch has two nodes. Equating these two expressions gives the result

$$\frac{L}{\Delta r} = 2\delta_N(L_T/A_F)/N_B. \tag{26}$$

Substituting into the limiting expression for the propagation constant of the mesh (Eq. 25) gives the relation of R and r.

$$R = \frac{\Gamma}{\sqrt{\tau}} r \tag{27}$$

$$\Gamma_m = \Gamma/\sqrt{\tau}. \tag{28}$$

The tortuosity factor τ is

$$\tau \triangleq \frac{\delta_N}{\delta_B} \frac{N_B}{2} \Big/ \left(\delta_N \frac{L_T}{A_F}\right)^2. \tag{29}$$

Substituting in the differential Eq. 23 now gives a differential equation of the same form as that of the disk model. Later, we determine τ for model networks and muscle fibers and discuss its physical meaning.

Analysis of the Admittance

It is necessary to analyze the current flow in the tubular system as well as the spread of potential, since most of the measurements of its electrical properties are really measurements of the contribution of the tubular network to the admittance of the muscle fiber. The admittance of the T-system also represents the largest part of the load on the action potential and so analysis of the admittance is needed to understand the propagation of the action potential.

The admittance of fundamental interest is that of an opening of the tubular system, but this can be derived from the admittance at a node of one inward radial branch. This admittance is (from Eq. 1 and 2)

$$\mathbf{y}_{n,k} \triangleq \frac{\mathbf{i}^-_{n,k}}{\mathbf{U}_{n,k}} = \mathbf{y}_{11}^{(k)} + \mathbf{y}_{12}^{(k)} \frac{\mathbf{U}_{n-1,k}}{\mathbf{U}_{n,k}}. \tag{30}$$

The random variable $\mathbf{Y}_n$ describes the admittance of the entire shell at index n. The expected value of $\mathbf{Y}_n$ is

$$E\{\mathbf{Y}_n\} = E\left\{\sum_k \mathbf{y}_{n,k}\right\} = \frac{2\pi(n - \frac{1}{2})\Delta r}{\delta_B} E\left\{\mathbf{y}_{11}^{(k)} + \mathbf{y}_{12}^{(k)} \frac{\mathbf{U}_{n-1,k}}{\mathbf{U}_{n,k}}\right\}. \tag{31}$$

As before, the sum over k is taken as the expected value times the number of radial branches per shell.

To proceed with the analysis, it is again necessary to take the mean or expected value of the admittance of a shell and try to relate that admittance to the mean electrical and morphometric parameters of the T-system. An interesting part of the previous analysis was the statistical argument (given in Appendix I) which allowed the estimation of the mean value of the admittance in terms of *only* the mean value of the electrical and morphometric parameters. In general, of course, such is not possible; the expected value of a function of a random variable depends on the entire distribution of the variable; in particular, it depends on the variance (and higher moments) as well as the mean value of the random variable. The mean value of the admittance is an example of the general case and can only be written as

$$E(\mathbf{Y}_n) = Y_n(1 + \epsilon_n),$$

or

$$E(\mathbf{Y}_n) = \frac{2\pi(n - \frac{1}{2})\Delta r}{\delta_B}\left(y_{11} + y_{12}\frac{U_{n-1}}{U_n}\right)(1 + \epsilon_n), \tag{32}$$

where Y_n is defined implicitly as the expected value of Y_n *if* $\epsilon_n = 0$. The error term ϵ_n, a measure of the effect of the shape of the distribution, is

$$\epsilon_n = P_{AB}\sigma_{AA}\sigma_{BB}/Y_n, \tag{33}$$

where $A = y_{12}$, $B = U_{n-1}/U_n$, and the correlation coefficient and variances are defined as in Appendix I. Although it is not possible with the data available to evaluate the correlation coefficient and variances, nonetheless, one can proceed on the assumption that they are quite small. The correlation coefficient measures the effect of the variance in one branch admittance on the voltage at a node adjoining that branch. Since the voltage is determined by the properties of the entire mesh, the variance of a single branch is likely to have a small effect. Furthermore, the variances themselves should be much smaller than the average values. Thus, it seems justified to ignore the error term.

Eq. 32 then serves as the fundamental relation between the admittance and the potential

$$U_n = \frac{1}{\rho}\frac{U_{n-1}}{(1 - \tilde{y}_n/y_{11})}, \tag{34}$$

where $\tilde{y}_n$ is the input admittance at the outer end of a radial branch n shells from the center.

$$\tilde{y}_n \triangleq \frac{\delta_B Y_n}{2\pi(n - \frac{1}{2})\Delta r}. \tag{35}$$

A first-order nonlinear difference equation (a Riccati equation) for the admittance can then be written from Eq. 18 by considering Eq. 34 and the additional case where n is replaced by $n + 1$. Then, we have

$$1 - \frac{\tilde{y}_{n+1}}{y_{11}} = \frac{n + \frac{1}{2}}{n\rho(2 + \xi^2) - \rho^2(n - \frac{1}{2})(1 - \tilde{y}_n/y_{11})}. \tag{36}$$

This difference equation, being of first order, is itself a statement of the numerical procedure to construct or compute its exact solution. Starting with the initial condition $\tilde{y}_0 = 0$, the difference equation gives $\tilde{y}_1$; $\tilde{y}_1$ can then similarly give $\tilde{y}_2$; and in this manner each $\tilde{y}_n$ can be trivially and efficiently computed.

Solutions of the Difference Equation

The solutions of the difference equations for the potential and admittance are most efficiently evaluated by direct programming of the equations, since they specify an iterative process. The procedure for computing the admittance has already been

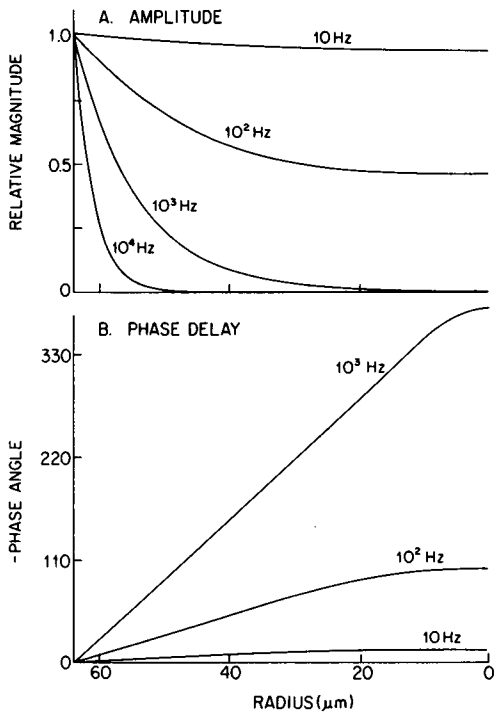

FIGURE 3 The radial distribution of potential in the mesh model. The difference Eq. 18 is solved directly for the parameters of an average muscle fiber (see Table II). *A* shows the relative attenuation in amplitude and *B* shows the delay or phase shift for sinusoidal voltages of different frequencies. The velocity of propagation of a point of constant phase (the phase velocity discussed by Carrier et al. 1966, p. 275) can be determined when the curves in *B* are approximately linear. The phase velocity is the angular frequency divided by the slope of the phase curve and is some 8 cm/s at 1,000 Hz, not greatly different from the radial propagation velocity of an action potential in the T-system.

specified; that for the potential is somewhat more complex since the difference Eq. 18 is second order. One boundary condition for the equation is specified in the center of the fiber, where the requirement that the admittance $\tilde{y}_0 = 0$ implies (from Eq. 34), that $U_1 = U_0/\rho$. Computation of the potential then proceeds by setting $U_0 = 1$, $U_1 = 1/\rho$ and using the difference equation to determine U_2 and so on. The potential on the outer edge of the T-system is then matched to the potential across the surface membrane and all the U_n scaled appropriately. The results of such a calculation are shown in Fig. 3.

The potential can also be written analytically (Pearson, 1960; Carrier et al., 1966, p. 105) in terms of an integral closely related to $I_0(n\xi)$

$$\psi_n = \frac{1}{\pi} \int_0^{\pi} \frac{\cosh n\xi t}{\sqrt{1 + \left(\frac{\xi}{2} \sin\theta\right)^2}} \, d\theta, \tag{37}$$

where

$$t = \frac{2}{\xi} \operatorname{arc\,sinh}\left(\frac{\xi}{2} \sin\theta\right). \tag{38}$$

ψ_n is an exact solution for the continuous limit and an accurate approximation in general, but another linearly independent solution (not presented in Pearson, 1960) is needed as well to satisfy our boundary condition and difference equation exactly. Although a complete asymptotic analysis of the integral expression might aid our understanding, we have only looked at a few special approximations. The most useful approximation for physiological purposes is the solution of the continuous limit of difference Eq. 23,

$$U_n = V_m \frac{I_0(n\xi)}{I_0(N\xi)} \tag{39}$$

where V_m is the surface member potential and N is the radial index of the surface of the fiber. This approximation is accurate, within 3.5% in magnitude, for frequencies up to 10 kHz in typical muscle fibers from the sartorius.

An approximate expression for the admittance can be derived that is quite useful: it has a simply physical interpretation and a specific relationship to the solutions of the continuous limit, namely the disk model. Furthermore, the error in the approximation is negligible under all physiological conditions. The critical step in the approximation is the definition and determination of the admittance $\tilde{y}_\infty$ of a network with radius much larger than its length constant. This parameter describes the admittance of a mesh in which potential does not spread to the center of the network, but drops essentially to zero within an outer annulus. There will always be such a limiting admittance, since Eq. 36 describes a sequence that increases, while the step size (the difference between $\tilde{y}_n$ and $\tilde{y}_{n+1}$) decreases. Thus, one can determine $\tilde{y}_\infty$ by setting $\tilde{y}_n = \tilde{y}_{n+1} = \tilde{y}_\infty$

$$\tilde{y}_\infty = \frac{\xi}{2\rho}\left[\sqrt{4 + \xi^2} - \xi(1 - 1/\xi_0^2)\right] Y_{T0} \coth \Gamma L, \tag{40}$$

where ξ is defined in Eq. 19 and

$$\xi_0 = \lim_{\Gamma L \to 0} (\xi/\Gamma L) = (N_B \delta_B / 2\delta_N)^{1/2}. \tag{41}$$

The solution to the difference equation for the admittance in the continuous limit is known from the previous work on the disk model (Adrian et al., 1969*a*) and so we construct a heuristic approximation that behaves correctly both for the $\xi \to 0$ and the $\xi \to \infty$ case (provided n is large enough; in our case $n > 20$).

$$\tilde{y}_n = \tilde{y}_\infty \frac{I_1(n\xi)}{I_0(n\xi)}, \; n > 20. \tag{42}$$

Rather than discuss the approximation analytically, it seems best simply to compare it with the exact numerical solution over the range of physiological interest. For the

parameters of a typical muscle fiber (see Results), at all frequencies the error in the magnitude of the admittance is less than 2% and the error in the phase of the admittance is less than 1% for fibers of radius $N = 20$ or larger (i.e., roughly 10 μm).

To complete the derivation, it is simply necessary to write the admittance formula in terms of morphometric parameters. The index variable $n\xi$ can be determined from Eq. 24 and can be related to specific properties of the tubular system by Eq. 28, 29, and 5. The variable ξ is defined in Eq. 19. The tubular network in a unit length of fiber has $(2\pi r - 0.5\Delta r)/\delta_B\sigma \simeq 2\pi r/\delta_B\sigma$ radial branches which form tubular openings, where σ is the sarcomere length. The tubular admittance in a unit length of fiber $y_T(r, j\omega)$ is then

$$y_T(r, j\omega) = \frac{2\pi r}{\delta_B\sigma}\tilde{y}_\infty \frac{I_1(\Gamma_m r)}{I_0(\Gamma_m r)}. \tag{43}$$

When the branch length is small compared to the length constant of the mesh, the expression approaches that for the continuous limit

$$y_T(r, j\omega) \sim 2\pi r \frac{V_T}{V_F}\Gamma_m \frac{\tau}{R_L}\frac{I_1(\Gamma_m r)}{I_0(\Gamma_m r)}. \tag{44}$$

The region of validity of this latter expression depends critically on the specific electrical parameters, morphometric parameters, and frequency and so cannot be easily described in general. However, in the next section we will see that the region of validity can be described in a general way by a physical argument.[4]

Physical Meaning of the Admittance Equation

An appealing feature of the solution (Eq. 43) of the mesh model is that it allows a simple physical interpretation of the admittance of the T-system (Fig. 4). We shall see that for large tubular length constants the lumen of the tubules is practically isopotential and so the admittance can be represented as a simple circuit. For a range of small length constants, the admittance behaves like that of a disk of T-system with significant decrement of potential in the radial direction. For a range of smaller length constants, the admittance is affected by the finite density of branching. Finally, for very small length constants, the admittance is simply that of the surface tubules in parallel.

---

[4] Although the derivation of Eqs. 43 and 44 assume networks enclosed in a boundary which is, on the average, circular, muscle fibers are usually irregular. The correct generalization to the irregular case is important. The factor $2\pi r$ in Eq. 43 and related equations obviously generalizes to the fiber circumference or boundary length B_F. The radial dimension within the argument of the Bessel functions in Eqs. 43 and 44 generalizes in a different manner, as can be seen by studying the case where $\Gamma_m a$ is small. Then, the T-system admittance must scale with the cross-sectional area of the fiber (see subsequent discussion). Thus, when the fiber is not circular, the radial coordinate within the Bessel function is replaced by $2A_F/B_F$. Numerical simulations of square, rectangular, and hexagonal networks have been performed (see Mathias, 1975) and it has been shown that Eq. 43, with the above definitions of "radius," is a surprisingly good model of the different geometries.

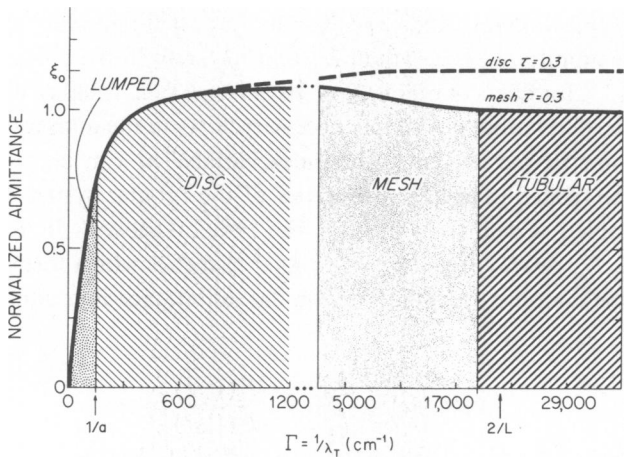

FIGURE 4 A plot of the normalized admittance vs. the tubular propagation constant. The variables and regions are defined in the text. The fiber radius is 65 μm, the specific circuit parameters are taken from Table II, and the morphometric parameters from Table I. The dashed line is computed from the disk model with the indicated tortuosity factor. The solid line is computed from the mesh model with the same tortuosity factor.

The admittance of the T-system depends on the properties both of an individual tubule and of the geometry of the tubular mesh. To isolate the effects of the geometry, it is best to study the properties of a normalized admittance $\tilde{y}_n/Y_{TO}$, the input admittance of a radial branch at an opening to the tubular system, defined in Eq. 42, divided by the characteristic (input) admittance of a single tubule, defined in Eq. 6:

$$\frac{\tilde{y}_n}{Y_{TO}} = \left(\frac{\tilde{y}_\infty}{Y_{TO}}\right) \frac{I_1(\Gamma_m r)}{I_0(\Gamma_m r)} \tag{45}$$

The first factor on the right side is called the mesh factor since it is most important in the region of short length constants, where the properties of the mesh are most important. The mesh factor is independent of Y_{TO}, since $\tilde{y}_\infty$ itself is proportional to Y_{TO} (see Eq. 40). The second factor is called the disk factor since it is most important in the region of long length constants, when the mesh behaves like a disk.

Fig. 4 shows the normalized admittance as a function of the tubular length constant or propagation constant. While this is the natural independent variable for analysis, it is important to remember that changes in frequency, conductance of the wall of the tubule, resistivity of the tubular lumen, or in the surface-to-volume ratio of the tubules can be analyzed from the figure and the definition of the propagation constant (Eq. 5). The line is the normalized admittance computed from Eq. 45. In the lumped region the mesh factor is constant while the disk factor is proportional to the effective radius, $\Gamma_m a$. Therefore at fixed radius, the normalized admittance is proportional to Γ_m. In this region the disk factor can be approximated by the first term in its expansion (see Fig. 5). Hodgkin and Nakajima (1972*a*,*b*; see Fig. 10 below) have shown that the "low-frequency" capacitance of a muscle fiber is linearly related to fiber radius and so

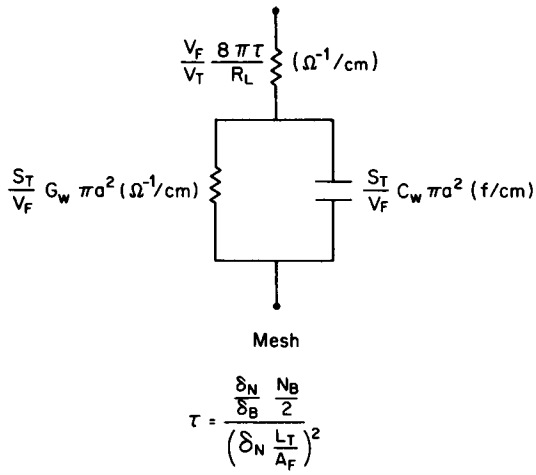

FIGURE 5 Lumped approximation valid for conditions of little radial decrement in potential within the tubular system. The variables are defined in the text. The circuit is valid in the lumped region identified in Fig. 4.

there is experimental evidence that at low frequencies the admittance of the T-system is in the lumped region.

For smaller values of the tubular length constant, the potential in the lumen of the tubules decrements significantly in the radial direction so the plot of the normalized admittance bends over towards a horizontal asymptote. In this disk region the mesh factor remains constant, but the disk factor approaches unity. When the disk factor is essentially unity, there is essentially no potential change in the center of the mesh. The network behaves like a disk of infinite radius, which would have a normalized admittance ξ_0. The normalized admittance is approximately independent of tubular length constant and fiber radius, a situation found experimentally in the T-system of muscle fibers during the foot of an action potential (Hodgkin and Nakajima, 1972*a*,*b*; see Fig. 10 below).

At still shorter length constants, the normalized admittance decreases from its maximum value (something less than ξ_0) to its eventual limiting value of unity. In this mesh region the disc factor is unity, but the mesh factor is decreasing. Finally, at very high frequencies or short length constants, the tubular system behaves as a set of tubules in parallel, since decrement of potential in the tubular lumen is so steep that essentially no current reaches the first node at which the tubular system branches. In this tubular region the disk factor remains unity, and the mesh factor has reached its limiting value of unity as well. The normalized admittance is independent of frequency or length constant, but of course the physical admittance does depend on these independent variables. It may seem surprising that the mesh factor should decrease with increasing frequency, but that is simply a consequence of the amount of tubular membrane available for current flow. At intermediate frequencies, current can flow across the walls of both types of branches of the tubular system (Θ branches and radial

branches). But at higher frequencies current can flow only across the walls of those radial branches lying just under the surface of the fiber. Thus, as frequency increases, there is less tubular membrane available for current to cross and so the normalized admittance decreases.

The Equivalent Circuit of the Tubular System in the Lumped Region

The expansion of y_T for small $\Gamma_m a$ is

$$\frac{1}{y_T} = \frac{1}{8\pi}\frac{1}{V_T/V_F}\frac{R_L}{\tau} + \frac{1}{\pi a^2}\frac{1}{S_T/V_F}\frac{1}{G_w + j\omega C_w}, \tag{46}$$

which describes the properties of the lumped equivalent circuit shown in Fig. 5.

Restricted Mesh Model

The analysis presented up to this point has assumed uniform properties of the T-system everywhere in the cross-section of the fiber. Other experimental findings however, suggest some nonuniformity in the structure of the T-system. Huxley and Taylor (1958: Fig. 3) found the current from an extracellular microelectrode elicited contraction only when applied to specific spots or regions widely separated at the Z line. If that technique allows the identification of every tubular opening, the circumferential spacing between the openings δ_s is considerably greater than the average branch spacing δ_B. Such wide spacings might restrict current flow into the tubular system, as suggested by Peachey and Adrian (1973). The wide spacing of openings could then be a morphological basis for the access resistance needed if the classical disk model is to produce an action potential with reasonable shape and conduction velocity (Adrian and Peachey, 1973).

We consider a nonuniform mesh, with spacing of the surface openings of the T-system δ_s different from the branch spacing δ_B in the interior. Each surface branch is assumed to connect to a number of inner branches (δ_s/δ_B) and, by circular symmetry, the admittance at each inner branch is given by $\tilde{y}_n$ defined in Eq. 42. The admittance of the entire restricted mesh y_{rm} (in a unit length of fiber) can be determined by an equation from two-port theory (Ghausi and Kelly, 1968, p. 24) for the impedance of a transmission line (here a surface branch) terminated in an arbitrary impedance.

$$y_{rm}(a,j\omega) = \frac{y_T + \frac{2\pi a}{\delta_s \sigma} Y_{TO} \tanh \Gamma L}{1 + y_T \frac{\tanh \Gamma L}{(2\pi a/\delta_s \sigma) Y_{TO}}}, \tag{47}$$

where y_T is the admittance, defined by Eq. 43, of the central part of the T-system. Note that the morphological and specific electrical properties of the central mesh and outer tubules need not be the same, although in the absence of contrary information we treat them as such. In the low-frequency case the restricted mesh equation becomes

$$y_{rm} \rightarrow \frac{y_T}{1 + r_a y_T}; \text{ small } \Gamma L, \tag{48}$$

where

$$r_a = \frac{\delta_s \sigma}{2\pi a} L r_{iT}. \tag{49}$$

Thus, the access model introduced by Peachey and Adrian approximates Eq. 47 over some range of length constants, and our analysis relates the parameters of the access model to the fundamental parameters of the tubules at the surface of the fiber.

METHODS

The preparation used in these experiments is the sartorius muscle of the frog *Rana pipiens*. The electronic apparatus is essentially that described by Valdiosera et al. (1974*a*). On occasion the voltage microelectrode was shielded as well as the current microelectrode. This shielding reduced the imaginary part of the extracellular potential essentially to zero, but it reduced the real part of the extracellular potential only by a factor of two. This reduction left an extracellular potential of the same order of magnitude as that found previously and so shielding was not routinely employed around the voltage electrode. The Ringer solution is described in Valdiosera et al. (1975*a*).

The procedure for the experiments was quite different from that previously described since it was designed to minimize the size of three-dimensional effects. Electrodes were inserted at a separation of 100 μm and the impedance of the fiber was measured in the frequency range 1–10,000 Hz. The low-frequency length constant was measured by making repeated impalements at a number of electrode separations, at least three, often four. The diameter was computed assuming R_i = 169 Ω-cm (Hodgkin and Nakajima, 1972*a*).

RESULTS

In this section the mesh model of the tubular system is fit to new data on the impedance of muscle fibers in normal Ringer solution and to previously published impedance data (Valdiosera et al., 1974*c*) and transient data (Hodgkin and Nakajima, 1972*a*,*b*). Some new morphometric measurements are presented but, for the most part, the morphometric data is that of Mobley and Eisenberg (1975) and Eisenberg and Peachey (1975). We are grateful to the above authors for making their data available to us in numerical form, in some cases before publication.

Table I gives the morphometric parameters and defines the morphometric symbols used throughout this paper. It is most important to note that the parameter values are distinctly different from the parameters of model networks previously used to describe the T-system. The parameters taken from Mobley and Eisenberg (1975) are marked STER to indicate that they were measured with stereological techniques; the data from Eisenberg and Peachey (1975) are marked HVEM to indicate they were measured in micrographs of thick sections taken with a high-voltage electron microscope. The spacing between the openings of the tubular system δ_s is estimated from Huxley and Taylor (1958). Values of the spacing between nodes δ_N and between branches δ_B were measured from electron micrographs of thick sections of frog sartorius muscle

TABLE I

MORPHOMETRIC PARAMETERS OF THE T-SYSTEM

Parameter	Symbol	Value	Units	Method
Surface of tubule per unit volume of fiber	S_T/V_F	2.2×10^3	cm^{-1}	STER
Surface of tubule per unit cross sectional area of fiber	S_T/A_F‡	0.59	—	STER
Surface of tubule per unit of volume of tubule	S_T/V_T	6.9×10^5	cm^{-1}	STER
Volume of tubule per unit volume of fiber	V_T/V_F	3.2×10^{-3}	—	STER
Length of tubule per unit cross sectional area of fiber	L_T/A_F‡	2.4×10^4	cm^{-1}	HVEM
Number of branches per node	N_B	3.2	—	HVEM
Branch length	L	9.0×10^{-5}	cm	HVEM
Branch spacing*	δ_B‡	$8.3(\pm 0.2) \times 10^{-5}$	cm	Text (HVEM)
Node spacing*	δ_N‡	$1.03(\pm 0.2) \times 10^{-4}$	cm	Text (HVEM)
Spacing of openings of T-system	δ_s‡	5×10^{-4}	cm	Huxley and Taylor
Tortuosity factor	τ‡	0.32	—	Text

*Parentheses enclose SEM, n = four muscles.

‡These parameters will in theory change with sarcomere spacing; the data presented here were measured in fibers with a sarcomere spacing of 2.8–3.0 μm.

kindly provided by Drs. B. Eisenberg and L. D. Peachey. The construction described previously (see Fig. 2) was applied to 11 muscle fibers from 4 muscles, between 3 and 12 shells being defined in each fiber. All the fibers were irregular and in one case the construction was completed just within a corner of the fiber. It is interesting that the apparent spacing between locations where the tubules approach the surface is 1 μm, much less than reported by Huxley and Taylor.

Fig. 6 shows the best fit of the mesh and restricted mesh model to the impedance data collected from two fibers at a sarcomere length of 2.5 μm. The points are the experimentally measured phase shift, namely the normalized delay between sinusoidal current injected with one microelectrode and the voltage recorded nearby (100 μm distant) with another microelectrode. Measurements of the magnitude of the impedance were routinely made in other experiments and could be fit by the circuit models and parameters reported here. They are not presented, however, since they contain only redundant information not necessary to determine the equivalent circuit or its parameter values. Indeed, the magnitude data is not very useful since the errors in its measurement are larger than those in the measurement of phase in the apparatus of

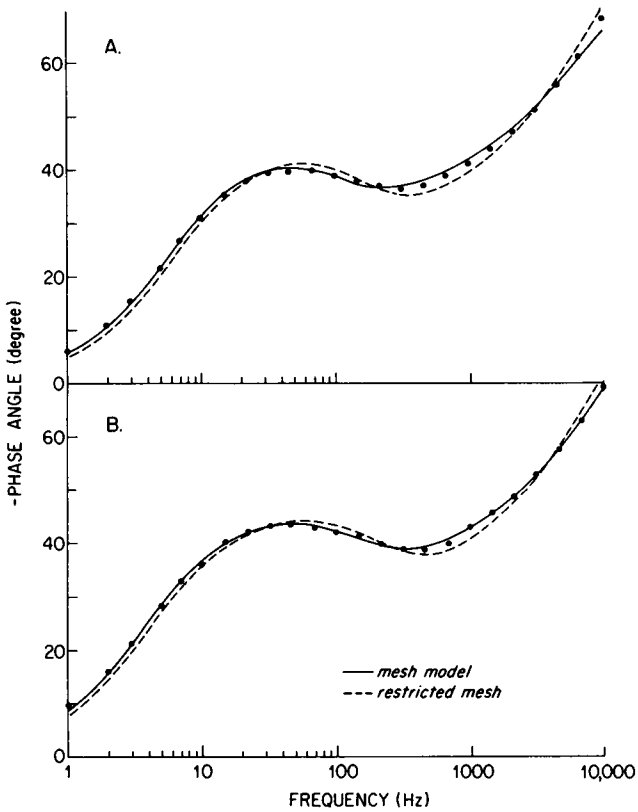

FIGURE 6 The phase angle of the impedance of frog skeletal muscle fibers measured at an electrode separation of 100 μm. The solid line is the best fit of the mesh model, the dashed line is the best fit of the restricted mesh model.

Valdiosera et al. (1974*a*). The phase data shown have been corrected for measured experimental errors and the theoretical curves have been fit to the data as described previously (Valdiosera et al., 1974*a,b,c*). Eq. 43 or 47 was used to describe the admittance of the T-system; the T-system admittance was added to the admittance of the surface membrane and from that sum the impedance of a one-dimensional cable, representing the one-dimensional properties of the muscle fiber, was calculated. At the electrode separations of 100 μm used here, the three-dimensional effect was negligible and therefore was not included. This is the procedure described by Valdiosera et al. (1974*b*) in their Eqs. 1, 2, and 5. Table II summarizes the results from five fibers. r_i and $\underline{r}$ are the internal longitudinal resistance and DC membrane resistance of a unit length of fiber determined from measurements of the magnitude of impedance at 1 Hz. The R_{test} is an objective measure of fit, giving the percent deviation between theory and experiment. The parameters C_w, C_m^* and R_L were determined by curve fitting to the phase data. All other parameters were determined by independent measurements and held constant during the curve-fitting procedure. The value of the

TABLE II

CIRCUIT PARAMETERS IN NORMAL RINGER SOLUTION, $\sigma = 2.5\ \mu m$

				Mesh				Restricted mesh			
Fiber	$\underline{r}$	r_i	a	C_m^*	C_w	R_L	R_{test}	C_m^*	C_w	R_L	R_{test}
	$10^4\ \Omega$-cm	$\mu\Omega/cm$	μm	$\mu F/cm^2$	$\mu F/cm^2$	Ω/cm	%	$\mu F/cm^2$	$\mu F/cm^2$	Ω/cm	%
210-1	8.7	2.70	45	1.1	1.1	180	2.3	1.3	1.0	120	2.0
211-1	20.6	3.35	40	1.0	1.8	120	1.0	1.3	1.4	80	4.3
211-2	20.6	4.06	36	1.0	1.7	120	0.8	1.3	1.4	80	4.3
211-3	21.2	2.75	44	1.2	1.4	90	1.0	1.6	1.1	70	2.6
216-1	17.2	3.26	41	1.0	1.2	170	1.6	1.2	1.0	110	2.8
Mean			41	1.1	1.4	136	1.3	1.3	1.2	92	3.2
SEM			4	0.1	0.1	17		0.1	0.1	10	

The radius is computed from an assumed internal resistivity $R_i = 169\ \Omega$-cm. The sarcomere length is $2.5\ \mu m$.

surface capacitance C_m^* is marked with an asterisk to indicate that the area of membrane used in its calculation is hypothetical, determined by assuming a smooth, unfolded surface membrane, whereas the real surface membrane is known to include folds and pockets often called caveolae (Dulhunty and Franzini-Armstrong, 1975). The circuit values presented in Table II should be calculated from morphometric and electrical measurements at the same sarcomere length. However, in the absence of such data, scaling is necessary. We scale the resistivity of the lumen of the tubules by scaling the tortuosity factor linearly with sarcomere length, as implied by Eq. 29: in a fiber that has volume independent of sarcomere length $\delta_N(L_T/A_F)$ will vary as the square root of sarcomere length. We do not choose to scale the capacitances nor analyze their relative values since their dependence on sarcomere length may be more complex. It is of interest that the restricted mesh model (with the value of $\delta_s = 5\ \mu m$

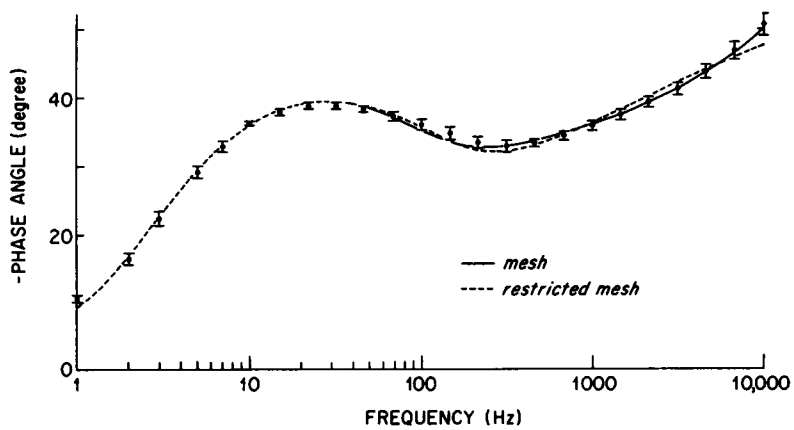

FIGURE 7 The phase angle of the input impedance of frog skeletal muscle fibers. The data is that of Valdiosera et al. (1974*c*) taken from 12 fibers in their 1 CCCP solution. Each point is the mean phase measured at that frequency. The standard error of the phase is indicated.

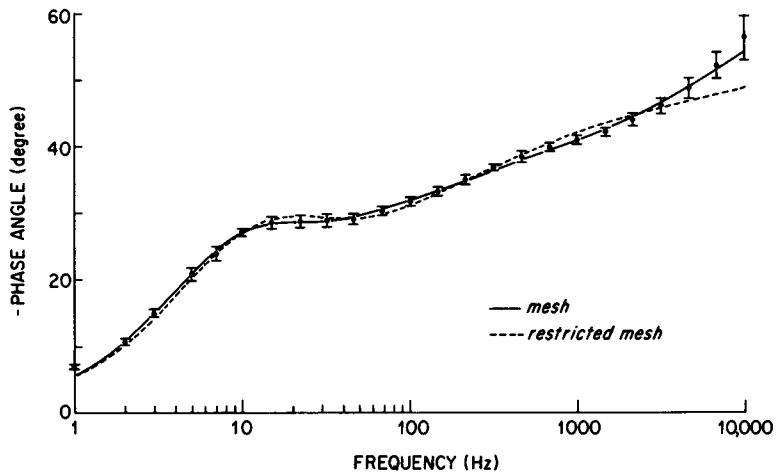

FIGURE 8 The phase angle of the input impedance of frog skeletal muscle fibers. The data is that of Valdiosera et al. (1974*c*) taken from 10 fibers in their $\frac{1}{8}$ CCCP solution. Each point is the mean phase measured at that frequency. The standard error of the phase is indicated.

from Huxley and Taylor, 1958) does not fit the experimental data nearly as well as the mesh model itself.

Figs. 7 and 8 and Table III present the data of Valdiosera et al. (1974*c*) from solutions of different conductivity identified in the original paper. The points here represent the mean data from a number of muscle fibers. It is more difficult to distinguish between the fit of the restricted mesh and mesh models, probably because these data include a significant three-dimensional effect that adds a degree of freedom to the curve-fitting procedure and thus reduces the accuracy of the best-fit circuit parameters. The difference between the circuit values for muscle fibers in normal Ringer solution shown in Table III and those shown in Table II is probably the result of biological variation, except for C_m^*, which is significantly affected by three-dimensional effects.

Fig. 9 illustrates the variation of luminal resistivity R_L with the resistivity of the bathing solution R_B. The solid straight line describes the case of equal resistivity of the bathing and luminal solution, the case expected to apply, since the lumen of the

TABLE III

CIRCUIT PARAMETERS IN SEVERAL SOLUTIONS, $\sigma = 2.5\,\mu m$

Solution	Mesh				Restricted mesh			
	C_w	C_m^*	R_L	R_{test}	C_w	C_m	R_L	R_{test}
	$\mu F/cm^2$	$\mu F/cm^2$	Ω-cm	%	$\mu F/cm^2$	$\mu F/cm^2$	Ω-cm	%
A: Ringer	1.07	0.73	148	1.2	0.90	1.61	116	1.5
E: 1 CCCP	1.23	0.85	281	1.0	1.03	1.65	200	1.5
F: $\frac{1}{2}$ CCCP	0.99	0.73	474	1.2	0.83	1.33	346	1.4
G: $\frac{1}{4}$ CCCP	1.28	0.82	990	1.7	1.00	1.43	704	1.5
H: $\frac{1}{8}$ CCCP	1.44	1.33	1263	1.1	1.15	1.86	834	2.2

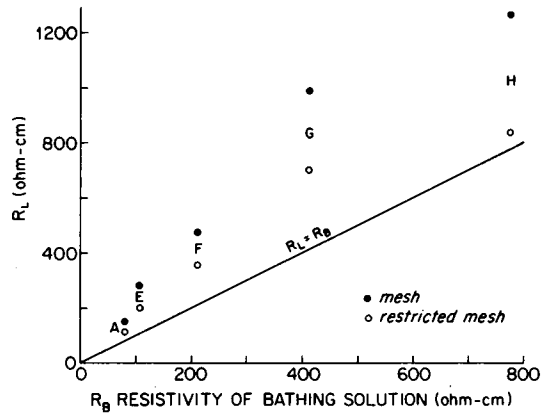

FIGURE 9 A plot of the resistivity of the lumen vs. the resistivity of the bathing solution. Note the different scales on the abscissa and the ordinate. The location of the points is determined from measurements of the morphometric parameters of muscle fibers and the parameters of the mesh and restricted mesh model that produce the best fit to the experimental phase data. The straight line shows the relation expected if the resistivity of the lumen equaled the resistivity of the bathing solution. It should be emphasized that there are no parameters available to arbitrarily adjust the slope of the line or the location of the points.

T-system is thought to be in diffusional equilibrium with the bathing solution. The points do not fall around this line, but are consistently above it. It seems to us that the most likely explanation of this deviation is an error in the morphometric measurements used to computer R_L, particularly since the derived value R_L depends on the square of L_T/A_F.[5] For example, if the morphometric parameters of Peachey (1965) are used to describe tubules of elliptical cross section 800 × 260 Å (and the node spacing and sarcomere length are as reported in Table I), the tortuosity factor is about 0.09. The resistivity of the lumen of the tubules, determined by fitting the impedance data and using Peachey's morphometric parameters, is about 30% of that reported in Tables II and III. Thus, if Peachey's morphometric parameters and the corresponding tortuosity factor were used, the resistivity of the lumen would appear to be much less than that of the bathing solution!

Up to this point we have examined the dependence of the admittance of a muscle fiber on the propagation constant, Γ_m, of the tubular system by varying the frequency of applied sinuosidal currents. Another independent variable that determines the admittance of the tubular system is the fiber radius, and so Hodgkin and Nakajima (1972*a*,*b*) studied the capacitance of muscle fibers as a function of fiber size. They measured the capacitance both from the voltage response to a step function of current

[5]The value for L_T/A_F was measured by Eisenberg and Peachey (1975) in 1.0-μm-thick sections observed in the high-voltage electron microscope. Thus, they measured the projection of the tubular length and their measurement would be an underestimate. Undulations of the tubules in the longitudinal direction would not be apparent in the projections measured and could cause as much as a 30% error at a sarcomere length of 2.9 μm.

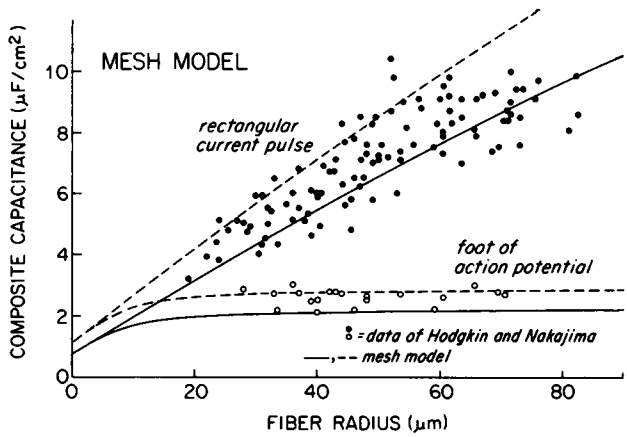

FIGURE 10 The variation of capacitance with fiber diameter. The data is from Hodgkin and Nakajima (1972*a*, *b*) and we thank the authors for providing the data in numerical form. The upper data describes the low-frequency capacitance determined from the application of rectangular pulses of current, and the lower data are the high-frequency capacitance, determined from the foot of the action potential. The theoretical curves are the predictions of the mesh model based on the circuit and morphometric parameters shown in Table II (the dashed line) or Table III (the solid line) for fibers in normal Ringer solution and the average of value of τ_f was 127 μs from Hodgkin and Nakajima, 1972*b*.

and from the foot of the action potential. The former estimates the total capacitance of the surface and tubular membranes; the latter measures the capacitance of the surface membrane and a small annulus of the tubular system. Fig. 10 compares the results of Hodgkin and Nakajima with the predictions of the mesh model, assuming that the specific properties and sarcomere length of the muscle fibers of *Rana temporaria* (used in their experiments) are the same as those of *R. pipiens*. The dashed line is calculated with the data shown in Tables I and II, the solid line with data shown in Tables I and III. The difference in the curves probably is mostly the result of biological variation, although the difference in the y-intercepts (the value of C_m^*) is undoubtedly influenced by the three-dimensional effects. The total capacitance curves were computed with Hodgkin and Nakajima, 1972*b*, Eq. 12, with the appropriate definition of the tortuosity factor (our Eq. 29). The effective capacitance during the foot of the action potential was computed with Eq. 16 of Hodgkin and Nakajima (1972*b*) with Y_T defined by $y_T/2\pi r$, where y_T is computed from Eq. 43 by replacing $j\omega$ with $1/\tau_f$.

DISCUSSION

Sensitivity to Assumptions

A number of assumptions used in the analysis of our data and derivation of the mesh model may introduce significant error. The most important assumption in the analysis of the data is that the circuit elements of the circuit model are relatively pure and can be described by resistors and capacitors. It is now known that the capacitance

of nerve and muscle fibers (Armstrong and Bezanilla, 1974; Schneider and Chandler, 1973) is voltage-dependent and so the assumption of pure circuit elements is bound to introduce some error. It is not possible to estimate this error without more precise data concerning the time dependence of the nonlinear capacitive currents found in muscle; however, consideration of the time scale reported suggests that the errors will be introduced at quite low frequencies. The time scale of the nonlinear capacitive currents in muscle is of the order of 10 ms. Errors would be expected then in the range of frequencies centered at 16 Hz. It is interesting that in this low-frequency range, most investigators have found a misfit to their impedance data (Schneider, 1970; Valdiosera et al., 1974*c*); however, the misfit has been shown to have little effect on the estimates of circuit parameters, since the estimates are rather insensitive to the low-frequency data. Thus, if the main effect of the nonlinear capacitive currents is confined to these low frequencies, the use of linear circuit elements probably does not introduce too much error. On the other hand, it must be kept in mind that there may be other properties of the nonlinear capacitive currents, not well studied at present, that could more seriously affect our results.

The most important assumption in the derivation of our model of the tubular system is that the construction defined in Fig. 2 will allow the potential in a typical tubular system to be described as a function of only one spatial variable; in other words, the assumption that the potential spread is circularly symmetric. There are three cases where one must question the assumption: first, if the shape of the fiber is grossly asymmetric; second, if there are asymmetries within the branching of the T-system itself; and third, if the longitudinal three-dimensional structure of the T-system is significant. Mathias (1975) has conducted quite extensive numerical analyses of branching networks and has observed that the admittance of several rectangular networks is remarkably close to that of the mesh model presented here. One must suppose that this result is not a coincidence but rather reflects an underlying applicability of the present mesh model to tubular networks in noncircular fibers.

Assymmetries within the tubular network at any given Z-disk certainly exist and spoil circular symmetry. Electrical data is measured, however, from the tubules in many Z-disks, from many fibers, and so represent the properties of an average tubular network. Asymmetries in the tubular network can thus be important only if they persist along the length of most muscle fibers, and there is so far no reason to suppose they do.

The effect of the three-dimensional structure of the T-system is difficult to estimate or analyze. There are few morphometric data on the number of longitudinal connections between Z-disks but there are almost no numerical data describing the overall three-dimensional geometry of the tubular system. Therefore, consideration of this complication must be postponed until more anatomical data are available.

The Disk Model, the Mesh Model, and the Tortuosity Factor

Adrian et al. (1969*a*) constructed an electrical model of the T-system that includes some effects of the branching of the tubules. The tubular system was described as

a resistive medium uniformly distributed within the interior of a muscle fiber and isolated by a membrane from the sarcoplasm (see also Falk and Fatt, 1964). A correction factor, the tortuosity factor, was introduced to account for the different properties of a T-system made of branching tubules and one made of a uniform resistive medium. The tortuosity factor was computed for several models with fixed regular geometries. There was some ambiguity in the determination of the tortuosity factor, since the networks considered do not pack into the circular perimeter assumed elsewhere in the analysis, but the networks considered by Schneider (1970) do pack into such a perimeter and give the same results.

In a sense it is no longer necessary to consider model networks, since our expressions for the admittance and potential contain all the morphometric and electrical parameters necessary to specify the current flow and potential distribution within the network. It remains desirable, however, to consider specific networks of resistors to see if one can develop a physical understanding of the meaning of the expressions, and indeed of the tortuosity factor. It is also important to consider such special cases to check the validity of our formulae. Finally, it is particularly important to consider such special cases to persuade the reader of the validity and applicability of our general results.

In a qualitative analysis of the tubular system, two resistances, derived from the specific properties of the T-system, may be defined. The effective resistance R_{rad} (in ohms) to radial current flow i_r (in amperes) in a single Z-disk is defined so that the radial form of Ohm's law is valid:

$$\frac{\partial U}{\partial r} = \frac{1}{2\pi r} R_{\text{rad}} i_r. \tag{50}$$

The other resistance has been specified by Adrian et al. (in slightly different form) as a bulk resistivity $\hat{R}_L$ (in ohm-centimeters) of the T-system, defined with respect to the volume of the fiber, instead of the volume of the tubular lumen:

$$\hat{R}_L = \frac{R_L}{V_T/V_F}. \tag{51}$$

These definitions are closely related to Eq. 3 and 6 of Adrian et al. (1969*a*). We find it easier to consider the properties of a single Z-disk and so we consider the analogous resistance $\tilde{R}_L$ for a single Z-disk by dividing the bulk resistivity by the sarcomere spacing

$$\tilde{R}_L \triangleq \frac{R_L}{V_T/A_F} = \frac{r_{iT}}{L_T/A_F}, \tag{52}$$

where V_T/A_F is the volume of the tubular lumen in a unit area of Z-disk, L_T/A_F is the length of tubule in a unit area of Z-disk, and r_{iT} is the resistance of a unit length of tubular lumen. The resistance $\tilde{R}_L$ can be written in terms of the resistance of one tubular branch $R_b \triangleq Lr_{iT}$:

$$\tilde{R}_L = \frac{R_b}{L(L_T/A_F)}. \tag{53}$$

Thus, $\tilde{R}_L$ is the resistance of $L(L_T/A_F)$ tubules in parallel, which is just the number of tubules in L^2 area of Z-disk. The tortuosity factor defined by Adrian et al. is given by

$$\tau = \frac{\tilde{R}_L}{R_{\text{rad}}}. \tag{54}$$

The definition of $\tilde{R}_L$ can be misleading, however, since it might be taken to imply that the radial resistance will decrease as the volume of tubules in a fiber increases. Such indeed would be the case for both $\tilde{R}_L$ and R_{rad} if the volume is increased by adding to each shell tubules that increase the number of parallel paths for current flow. But such would not be the case for R_{rad} if the volume were increased by increasing the path length for current flow, keeping everything else constant. Thus, we are immediately aware that the relationship between R_{rad} and $\tilde{R}_L$ will be complex and will depend strongly on the geometric and morphometric properties of the tubular network.

Consider now two specific networks[6] shown in Fig. 11. The diamond model is divided into shells by constructing curves similar to those used in our derivation of the mesh model (see Fig. 2). The curves define δ_B which, for this model, is equal to $L/\sqrt{2}$. A unit cell is constructed that can be repeated to build the entire network and from such a cell average morphometric parameters can be directly determined. For this network the unit contains two branches of length L in a rectangle $\delta_N = \sqrt{2}L$ by $\Delta r = L/\sqrt{2}$ of area L^2. Thus, $L_T/A_F = 2/L$. The expression for the radial current in a shell of perimeter $2\pi r$ is

$$i_r = \frac{2\pi r}{\delta_N}\frac{2}{R_b}[U(r + \Delta r) - U(r)] = \frac{2\pi r}{R_b}\frac{\Delta U}{\Delta r}, \tag{55}$$

which, by comparison with the finite difference representation of Eq. 50 gives $R_{\text{rad}} = R_b$. Note the factor of $2/R_b$ in the center expression of Eq. 55 because there are two branches for radial current flow at each node.[7] The resistance $\tilde{R}_L$ can be deter-

[6]The derivation we have described applies to a wide variety of networks, namely to those networks in which each constructed shell is the same and in which each branch length is the same. It cannot be used, however, to analyze the "out-of-register squares" of Schneider (1970) or Fig. 11 (d) of Adrian et al. (1970). Those networks are equivalent to an hexagonal array with the laterally oriented branches being one half the length of the radially oriented branches, and the approach in the text assumes branches in all directions to have, on the average, the same length. Such networks can be analyzed by modifying the equations for current flow, but then the tortuosity factor would depend on the average branch length and probably the ratio of branch lengths in different directions. With the available morphological evidence it does not seem worthwhile to pursue this point further.

[7]The node spacing, δ_N, can be used here because we know the number of radial branches at each node. In the random case, however, it is necessary to use the branch spacing, δ_B, since there does not appear to be a direct method of determining the number of minus branches at each node.

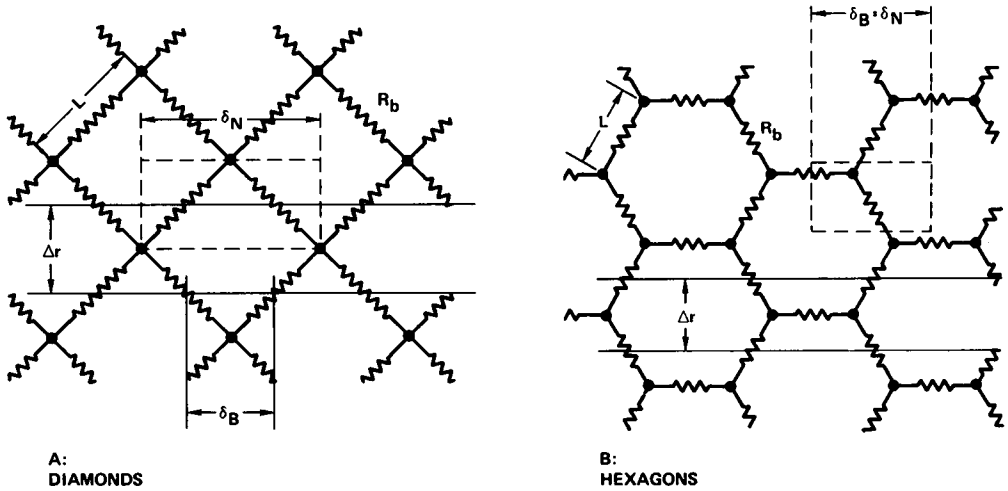

FIGURE 11 Two networks of resistors to illustrate the application of the mesh and disk model to specific circuits. The symbols are defined in the text.

mined from Eq. 53 and is $R_b/2$. The tortuosity factor defined by Eq. 29 of the mesh analysis can be determined from the morphometric parameters of the unit cell and is 0.5 for the diamond model. The ratio $\tilde{R}_L/R_{rad} = 0.5$ is thus equal to the tortuosity factor as we expect from our derivation and the definitions of Adrian et al.

The analysis can be extended to the case where the tubules are not taut. Imagine that the network is collapsed so that all dimensions are divided by p, but branch length L is kept constant. The morphometric parameter L_T/A_F is now $2L/(L/p)^2 = 2p^2/L$. Since the branch current does not change, and Δr still equals $2\delta_N$, the value of R_{rad} is unchanged. The value of R_L is changed, however, because the dimensions of the unit cell are reduced. We then have $\tilde{R}_L/R_{rad} = 1/(2p^2)$; the tortuosity factor is also $1/(2p^2)$. The tortuosity factor thus depends critically on the degree of tautness of the tubules. This dependence undoubtedly contributes to the difference between the value of τ in Table II and in Adrian et al. (1969*a*).

Next consider the hexagonal network shown in Fig. 11. The orientation shown was chosen so the constructed shells all have the same properties, as our analysis of a random mesh assumes; other orientations of hexagons do not have this property. This network is of particular interest since it has three branches per node and so is the closest approximation to the tubular system among deterministic networks. Even so, however, the morphometric parameters of the taut network shown in Fig. 11B are quite different from those of a muscle fiber. The average morphometric parameters can be determined from the unit cell which is a rectangle $\delta_N = \delta_B$ by Δr. The branch or node spacing alternates between two values; $\delta_N = \delta_B = 3L/2$ is the mean. The shell spacing $\Delta r = \sqrt{3}/2$. L_T/A_F is then $2/\sqrt{3}L$ and $\tilde{R}_L$ is $\sqrt{3}R_b/2$. The radial current is easily determined since the θ branches do not contribute to the radial

resistance:

$$i_r = \frac{2\pi r}{\delta_N} \frac{\Delta r}{R_b} \frac{\Delta U}{\Delta r} = \frac{2\pi r}{\sqrt{3} R_b} \frac{\Delta U}{\Delta r}. \tag{56}$$

Thus, $R_{rad} = \sqrt{3} R_b$ and $\tilde{R}_L / R_{rad} = 0.5$, again equal to the tortuosity factor of the mesh model. The computation of an untaut network of hexagons gives the same result previously described for untaut diamonds.

The previous examples illustrate the analysis of specific networks by the mesh model or by methods used in the derivation of the disk model of Adrian et al. (1969*a*). In a general case, such as the tubular system of skeletal muscle fibers, no specific network is known. All that is available to describe the network is a set of morphometric parameters. We now show how these morphometric parameters by themselves can define a revised disk model, which turns out to be identical to the continuous limit of the mesh model.

In any network the potential drop between adjacent shells of width Δr is the radial current times the resistance of a radial branch divided by the number of radial branches

$$\Delta U = \frac{i_r R_b}{2\pi r / \delta_B}. \tag{57}$$

A general definition of R_{rad}, analogous to Eq. 50, can thus be written without consideration of a tortuosity factor.

$$R_{rad} = \frac{R_b}{\Delta r / \delta_B}. \tag{58}$$

This definition requires, however, a general geometric construction (see Fig. 2) and analysis (see text near Eqs. 26 and 53) to define Δr in terms of morphometric parameters. Then,

$$R_{rad} = \frac{\delta_N^2 (R_b / L)(L_T / A_F)}{\zeta}, \tag{59}$$

where

$$\zeta \triangleq \frac{N_B}{2} \frac{\delta_N}{\delta_B}. \tag{60}$$

The differential equation for radial current in the disk model is derived by dividing Eq. 57 by Δr, substituting Eq. 59, and taking the limit as $\Delta r \to 0$.

$$\frac{\Delta U}{\Delta r} \to \frac{\partial U}{\partial r} = \frac{i_r}{2\pi r} \frac{\tilde{R}_L}{\tau}, \tag{61}$$

where $\tilde{R}_L$ is defined in Eq. 52 and τ in Eq. 29. The derivation is completed by introducing an equation for the conservation of current (Adrian et al., 1969*a*, Eq. 7).

The Tortuosity Factor

The tortuosity factor τ has been defined as the ratio of the bulk resistance $\tilde{R}_L$ to the effective radial resistance R_{rad}, although the above revised derivation suggests more natural definitions. Therefore, a physical interpretation of τ is best accomplished by first considering those resistances. $\tilde{R}_L$ has already been discussed and is simply the resistance of the parallel combination of all tubular branches in an area L^2 of Z-disk. One physical meaning of the radial resistance R_{rad} is shown in its definition (Eq. 50); however, the meaning of R_{rad} in terms of the network parameters is best considered by examining the numerator and denominator of Eq. 59 separately. The numerator is simply the number of tubules in an area δ_N^2 of Z-disk times the luminal resistance of one tubule. In other words it is the total resistance of a *series* combination of all the tubular branches in that area. The geometric factor ζ in the denominator of Eq. 59 can now be defined physically as the ratio of the total series resistance of the branches at a node divided by the effective radial resistance due to those branches. Since each of these quantities has a physical meaning, the geometric factor itself can be determined directly from specific networks. Indeed, that is one of the reasons for defining the geometric factor as we have. For example, in the diamond network in Fig. 11 there are two radial branches at each node, which are effectively in parallel. Thus,

$$\zeta = \frac{2R_b}{\frac{1}{2}R_b} = 4 \quad \text{(diamond network).} \tag{62}$$

In the hexagonal network in Fig. 11,

$$\zeta = \frac{\frac{3}{2}R_b}{r_b} = \frac{3}{2} \quad \text{(hexagonal network).} \tag{63}$$

The value of ζ can also be determined directly from its definition, with identical results. The definition of ζ also shows why the name geometric factor is appropriate; ζ depends only on the ratio of δ_N and δ_B and so is independent of the amount of tubular system and of the tautness of the tubular network.

The physical interpretation of $\tilde{R}_L$ and R_{rad} now permits a physical interpretation of the tortuosity factor, which can be written

$$\tau = \zeta\left\{\frac{\tilde{R}_L}{R_b(\delta_N^2/L)(L_T/A_F)}\right\} = \zeta/(\delta_N L_T/A_F)^2. \tag{64}$$

The tortuosity factor thus is composed of two terms, one the geometric factor already discussed, the other a morphometric factor, the ratio of the parallel resistance of the tubular branches in area L^2 to the series resistance of the tubular branches in area δ_N^2. This morphometric factor (the denominator on the right-hand side of Eq. 64) depends strongly on the degree of tautness in the network. For a general network in a closed boundary $\delta_N L_T/A_F$ changes in proportion to the change in dimension. The proportionality constant, however, is different for different networks. The dependence of $\delta_N(L_T/A_F)$ and the tortuosity factor on the deformation of a network can be

clearly displayed by rewriting Eq. 64 by using Eq. 26:

$$\tau = \frac{\zeta}{\left(\frac{L}{\Delta r}\frac{N_B}{2}\right)^2}. \tag{65}$$

The factor $L/\Delta r$ represents the length of tubule per unit distance in the radial direction, and is modified by $N_B/2$ and the geometric factor to make the tortuosity factor.

Eqs. 64 and 65 show the dependence of the tortuosity factor on all the dimensions of the network; however, neither explicitly includes the constraint that the total amount of tubular system in a muscle fiber stays constant when the dimensions change, and so they can be misleading if taken by themselves. Furthermore, in general Δr is not directly known but must be computed from morphometric parameters. Thus, in most respects Eq. 64 is the more general formulation.

Comparison with Previous Results

Our figures for the specific electrical properties of frog skeletal muscle fibers differ from those of, for example, Valdiosera et al. (1974*c*) for three reasons: (*a*) different morphometric parameters are used; (*b*) the mesh model is used to determine the expression and value for the tortuosity factor; and (*c*) the mesh model is used to describe the properties of the T-system. The different value of the resistivity of the lumen of the tubules is primarily a consequence of the different morphometric parameters and tortuosity factor. The different values of the specific capacitances are primarily a consequence of the different morphometric parameters. The parameters reported are not very sensitive to the discrete properties of the tubular mesh since these become important only at high frequencies and in solutions of low conductivity.

APPENDIX

In order to proceed beyond Eq. 15 of the text, it is necessary to evaluate several mathematical expectations similar to Eq. 17. We adopt the following nomenclature:

$$\begin{aligned}
E\{\mathbf{y}_{11}^m \text{ or } \mathbf{y}_{12}^m\} &\triangleq y_{11} \text{ or } y_{12},\\
E\{\mathbf{U}_{n,m}\} &\triangleq U_n,\\
E\{(\mathbf{y}_{11}^m - y_{11})^2\} &\triangleq \sigma_{11}^2,\\
E\{(\mathbf{y}_{12}^m - y_{12})^2\} &\triangleq \sigma_{12}^2,\\
E\{(\mathbf{U}_{n,m} - U_n)^2\} &\triangleq \sigma_n^2,\\
E\{(\mathbf{U}_{n,m} - U_n)(\mathbf{y}_{11}^m - y_{11})\} &= E\{\mathbf{U}_{n,m}\mathbf{y}_{11}^m\} - U_n y_{11} \triangleq \mu_{11}^n, \text{ and}\\
E\{(\mathbf{U}_{n,m} - U_n)(\mathbf{y}_{11}^m - y_{12})\} &= E\{\mathbf{U}_{n,m}\mathbf{y}_{12}^m\} - U_n y_{12} \triangleq -\mu_{12}^n,
\end{aligned} \tag{A1}$$

where the negative sign on the covariance in the last expression is due to the physical requirement that $y_{12} < 0$. Eq. 17 of the text can be written in general as

$$i_n^+ = E\{\mathbf{y}_{11}^m\mathbf{U}_{n,m} + \mathbf{y}_{12}^m\mathbf{U}_{n+1,m}\} = y_{11}U_n + \mu_{11}^n + y_{12}U_{n+1} - \mu_{12}^{n+1}. \tag{A2}$$

If we substitute expressions similar to Eq. A2 for the average currents i_n^- and i_n^θ, then the full expression for Eq. 15 of the text is

$$(n + \tfrac{1}{2})(y_{11} U_n + y_{12} U_{n+1}) + (n - \tfrac{1}{2})(y_{11} U_n + y_{12} U_{n-1})$$
$$-n(2 - N_B \delta_B / \delta_N)(y_{11} + y_{12}) U_n + (n + \tfrac{1}{2})(\mu_{11}^n - \mu_{12}^{n+1}) + (n - \tfrac{1}{2})(\mu_{11}^n - \mu_{12}^{n-1})$$
$$-n(2 - N_b \delta_B / \delta_N)(\mu_{11}^n - \mu_{12}^n) = 0. \quad \text{(A3)}$$

The covariances, for example μ_{11}^n, can be expressed as

$$\mu_{11}^n = P \sigma_{11} \sigma_n, \quad \text{(A4)}$$

where P is the correlation coefficient for $\mathbf{y}_{11}^m$ with $\mathbf{U}_{n,m}$. The correlation coefficient is expected to be much less than unity and the individual variances are much less than the mean values. Thus, the covariance terms can be neglected. An equation for the expected value can also be written with an exact argument. Eq. A3 specifies a combination of covariances and mean values of the potential that must equal zero. There are situations described by this equation in which the variance can be modified with a fixed average potential distribution. For example, networks with definite deterministic branch lengths but with random interconnections should have no variance in the admittance of individual branches; from Eq. A4 we see that the covariances would also be zero. This and similar situations can be described by Eq. A3 only if two separate expressions are individually equal to zero, one involving just the mean value of the potential, another involving just the covariances. Thus, either approximately or exactly, one can write

$$(n + \tfrac{1}{2}) U_{n+1} + (n - \tfrac{1}{2}) U_{n-1} - n(2 + \xi^2) U_n = 0, \quad \text{(A5)}$$

where

$$\xi^2 = -\frac{\delta_B}{\delta_N} N_B \left(\frac{y_{11}}{y_{12}} + 1 \right) > 0, \quad \text{(A6)}$$

since[8]

$$-y_{11}/y_{12} \cong \cosh \Gamma L > 1.$$

This expression for potential is analyzed in the text and is shown to have the approximate solution of a zero-order hyperbolic Bessel function when ξ is small.

Discussions and correspondence with W.K. Chandler and M. Schneider were most helpful in the development of our thoughts concerning the disk model. The perceptive criticisms of this work by R. H. Adrian and W. Almers provided much of the motivation for the treatment of a random network and the shell construction. We are grateful to our colleagues for the time and energy spent on these problems.

Dr. Mathias was a Fellow of Muscular Dystrophy Association and received support from National Science Foundation grant ENG7-11876 to Prof. N. Levan. Dr. Valdiosera was supported by the Los Angeles County Heart Association. The experimental work and computations were supported by a Muscular Dys-

[8]The random short-circuit admittances $\mathbf{y}_{11}$ and $\mathbf{y}_{12}$ represent functions of the random variables that describe the geometry and electrical properties of a single tubular branch (e.g., $\mathbf{L}$, $\mathbf{G}_w$, etc.). The evaluation of the expected value of the admittances requires a complete knowledge of the probability distribution function of these geometrical and electrical variables. In the absence of such knowledge we define y_{11} and y_{12} (see text, Eq. 3 and 4) by replacing the random variables with their respective mean values, a procedure that may introduce an error of a few percent.

trophy Grant and National Science Foundation grant MBS75-5500. We are grateful to J. Ramon and C. Clausen for their assistance in computer programming and to our colleagues, B. Eisenberg, R. Levis, and A. Peskoff, for their useful comments throughout the course of the work.

Received for publication 3 May 1976 and in revised form 29 September 1976.

REFERENCES

ADRIAN, R. H., W. K. CHANDLER, and A. L. HODGKIN. 1969*a*. The kinetics of mechanical activation in frog muscle. *J. Physiol. (Lond.)* **204**:207–230.

ADRIAN, R. H., L. L. CONSTANTIN, and L. D. PEACHEY. 1969*b*. Radial spread of contraction in frog muscle fibers. *J. Physiol. (Lond.).* **204**:231–257.

ADRIAN, R. H. and L. D. PEACHEY. 1973. Reconstruction of the action potential of frog sartorius muscle. *J. Physiol. (Lond.).* **235**:103–131.

ARMSTRONG, C. M., and F. BEZANILLA. 1974. Charge movement associated with the opening and closing of the activation gates of the Na channels. *J. Gen. Physiol.* **63**:533–552.

BARRY, P. H., and R. H. ADRIAN. 1973. Slow conductance changes due to potassium depletion in the transverse tubules of frog muscle fibers during hyperpolarizing pulses. *J. Membr. Biol.* **14**:243–292.

CARRIER, G. F., M. KROOK, and C. E. PEARSON. 1966. Functions of a Complex Variable. McGraw-Hill Book & Education Services Group, New York.

COSTANTIN, L. L. 1975. Contractile activiation in skeletal muscle. *Prog. Biophys. Mol. Biol.* **29**:197–224.

DESOER, C. A., and E. S. KUH. 1969. Basic Circuit Theory. McGraw-Hill, Inc., New York.

DULHUNTY, A. F., and C. FRANZINI-ARMSTRONG. 1975*a*. Variations in internal resistivity with sarcomere length in frog semitendinosus fibers. *Biophys. J.* **15**:130*a* (Abstr.).

DULHUNTY, A. F., and C. FRANZINI-ARMSTRONG. 1975*b*. The relative contribution of the folds and caveolae to the surface membrane of frog skeletal muscle fibers at different sarcomere lengths. *J. Physiol. (Lond.).* **250**:513–539.

EISENBERG, B., and L. D. PEACHEY. 1975. The network parameters of the t-system in frog muscle measured with the high voltage electron microscope. 33rd Annual Proceedings of the Electron Microscopy Society of America. G. W. Bailey, editor, Claitor's Publishing Division, Baton Rouge, La.

ENDO, M. 1966. Entry of fluorescent dyes into the sarcotubular system of frog muscle. *J. Physiol. (Lond.).* **185**:224–238.

FALK, G., and P. FATT. 1964. Linear electrical properties of striated muscle fibers observed with intracellular electrodes. *Proc. R. Soc. Lond. B. Biol. Sci.* **160**:69–123.

GHAUSI, M. S., and J. J. KELLEY. 1968. Introduction to distributed-parameter networks. Holt, Rinehart and Winston, Inc., New York.

GILAI, A. 1976. Electromechanical coupling in tubular muscle fibers. II. The resistance and capacitance of one transverse tubule. *J. Gen. Physiol.* **67**:343–367.

GONZALEZ-SERRATOS, H. 1966. Inward spread of contraction during a twitch. *J. Physiol (Lond.).* **185**: 20–21.

HODGKIN, A. L., and S. NAKAJIMA. 1972*a*. The effect of diameter on the electrical constants of frog skeletal muscle fibers. *J. Physiol. (Lond.).* **221**:105–120.

HODGKIN, A. L., and S. NAKAJIMA. 1972*b*. Analysis of the membrane capacity of frog muscle. *J. Physiol. (Lond.).* **221**:121–136.

HUXLEY, A. F., and R. E. TAYLOR. 1958. Local activation of striated muscle fibers. *J. Physiol. (Lond.).* **144**:426–441.

JACK, J. J. B., D. NOBLE, and R. W. TSIEN. 1973. Electric current flow in excitable cells. Clarendon Press, Oxford University Press, London, U.K.

MATHIAS, R. T. 1975. A study of the electrical properties of the transverse tubular system in skeketal muscle. Ph.D. Thesis in Engineering, University of California at Los Angeles.

MOBLEY, B. A., and B. EISENBERG. 1975. Sizes of components in frog skeletal muscle measured by methods of stereology. *J. Gen. Physiol.* **66**:31–45.

NAKAJIMA, S., Y. NAKAJIMA, and J. BASTIAN. 1975. Effects of sudden changes in external sodium concentration of twitch tension in isolated muscle fibers. *J. Gen. Physiol.* **65**:459–482.

NAKAJIMA, S., and J. BASTIAN. 1976. Membrane properties of the transverse tubular system in amphibian

skeletal muscle. *In* Electrobiology of Nerve, Synapses, and Muscle. J. P. Reuben, D. P. Purpura, M. V. L. Bennett, and E. R. Kandel, editors. Raven Press; New York.

PAPOULIS, A. 1965. Probability random variables and stochastic processes. McGraw-Hill, Inc., New York.

PEACHEY, L. D. 1965. The sarcoplasmic reticulum and transverse tubules of the frog's sartorius. *J. Cell. Biol.* **25**:209–231.

PEACHEY, L. D., and R. H. ADRIAN. 1973. Electrical properties of the transverse tubular system. *In* Structure and function of muscle. Vol. III. Physiology and Biochemistry. G. H. Bourne, editor. 2nd edition. Academic Press, Inc., New York.

PEACHEY, L. D., and B. EISENBERG. 1975. The T-system and striations of frog skeletal muscle are spiral. *Biophys. J.* **15**:253*a*. (Abstr.).

PEARSON, C. E. 1960. Integral representation for solutions of Bessel's difference equations. *J. Math. Phys.* **4**:287–292.

SCHNEIDER, M. F. 1970. Linear electrical properties of the transverse tubules and surface membrane of skeletal muscle fibers. *J. Gen. Physiol.* **56**:640–671.

SCHNEIDER, M. F., and W. K. CHANDLER. 1973. Voltage dependent charge movement in skeletal muscle: a possible step in excitation-contraction coupling. *Nature (Lond.).* **242**:244–246.

VALDIOSERA, R., C. CLAUSEN, and R. S. EISENBERG. 1974*a*. Measurements of the impedance of frog skeletal muscle fibers. *Biophys. J.* **14**:295–315.

VALDIOSERA, R., C. CLAUSEN, and R. S. EISENBERG. 1974*b*. Circuit models of the passive electrical properties of frog skeletal muscle fibers. *J. Gen. Physiol.* **63**:432–459.

VALDIOSERA, R., C. CLAUSEN, and R. S. EISENBERG. 1974*c*. Impedance of frog skeletal muscle fibers in various solutions. *J. Gen. Physiol.* **63**:460–491.